EFFECTS OF PARTICULATE MATTER ON ATMOSPHERIC PROPAGATION OF CO2 LASER RADIATION

David C. Smith, et al

United Aircraft Research Laboratories

Prepared for:

Office of Naval Research

30 July 1973

Unclassified

Security Classification

i

AD-775221

DOCUMENT CONTROL DATA - R&D

(Security classification of title, body of abstract and indexing annotation must be entered when the overall report is classified)

1. ORIGINATING ACTIVITY (Corporate author) United Aircraft Corporation Research Laboratories 400 Main Street, East Hartford, CT 06108	2a. REPORT SECURITY CLASSIFICATION Unclassified 2b. GROUP NA

3. REPORT TITLE

Effects of Particulate Matter on Atmospheric Propagation of CO_2 Laser Radiation

4. DESCRIPTIVE NOTES (Type of report and inclusive dates)

Final Report, July 1, 1972 to July 30, 1973

5. AUTHOR(S) (Last name, first name, initial)

Smith, David C., Brown, Robert T., Gebhardt, Frederick, G., Berger, Paul J.

6. REPORT DATE	7a. TOTAL NO. OF PAGES	7b. NO. OF REFS
July 30, 1973	64	18

8a. CONTRACT OR GRANT NO.	9a. ORIGINATOR'S REPORT NUMBER(S)
N00014-72-C-0469 b. PROJECT NO. NR c. d.	M-921503-3 9b. OTHER REPORT NO(S) (Any other numbers that may be assigned this report)

10. AVAILABILITY/LIMITATION NOTICES

11. SUPPLEMENTARY NOTES	12. SPONSORING MILITARY ACTIVITY
	Office of Naval Research Department of the Navy Arlington, Virginia

13. ABSTRACT

The influence of aerosols, or particulates, on thermal blooming and gas breakdown of 10.6 micron wavelength radiation has been measured. When particles are irradiated with high intensity pulsed CO_2 laser beams, gas breakdown is initiated and the plasma formed limits the propagation of the beam. Experimental measurements of the threshold for ionization of single particles electrodynamically suspended at the focus of a beam have been measured. For alumina particles the threshold was independent of particle size from 1 to 70 micron diameter and was 0.4 - 1 x 10^8 W/cm^2. The threshold was found to decrease with increasing background pressure, apparently the result of retardation of the particle vapor expansion. Streak photographs of the plasma expansion and schlieren studies are also reported. A theoretical analysis of solid particles laser radiation interaction indicates that the mechanism leading to breakdown is superheating of the particle material with subsequent ionization of the solid or of the material directly adjacent to the solid. Experiments were carried out to examine the thermal blooming of a cw CO_2 laser beam propagating in a carbon dust ladened gas used to simulate aerosols and this blooming was compared with that caused by a molecular absorber. Measurements were also made of the time required to heat single electrodynamically suspended particles to incandecence in a cw CO_2 laser beam; this time is a measure of the rate of energy absorption. Transient thermal blooming of a pulsed CO_2 laser beam was examined in the time regime where the laser pulse was comparable to the acoustic transit time across the beam, τ_a. The results show the advantage of reduced thermal distortion for laser pulses whose duration is short compared to τ_a.

DD FORM 1 JAN 64 1473

Security Classification

14. KEY WORDS	LINK A		LINK B		LINK C	
	ROLE	WT	ROLE	WT	ROLE	WT
Laser-Particle Interaction Atmospheric Propagation Gas Breakdown Threshold Transient Thermal Blooming CO_2 Lasers						

INSTRUCTIONS

1. ORIGINATING ACTIVITY: Enter the name and address of the contractor, subcontractor, grantee, Department of Defense activity or other organization *(corporate author)* issuing the report.

2a. REPORT SECURITY CLASSIFICATION: Enter the overall security classification of the report. Indicate whether "Restricted Data" is included. Marking is to be in accordance with appropriate security regulations.

2b. GROUP: Automatic downgrading is specified in DoD Directive 5200.10 and Armed Forces Industrial Manual. Enter the group number. Also, when applicable, show that optional markings have been used for Group 3 and Group 4 as authorized.

3. REPORT TITLE: Enter the complete report title in all capital letters. Titles in all cases should be unclassified. If a meaningful title cannot be selected without classification, show title classification in all capitals in parenthesis immediately following the title.

4. DESCRIPTIVE NOTES: If appropriate, enter the type of report, e.g., interim, progress, summary, annual, or final. Give the inclusive dates when a specific reporting period is covered.

5. AUTHOR(S): Enter the name(s) of author(s) as shown on or in the report. Enter last name, first name, middle initial. If military, show rank and branch of service. The name of the principal author is an absolute minimum requirement.

6. REPORT DATE: Enter the date of the report as day, month, year, or month, year. If more than one date appears on the report, use date of publication.

7a. TOTAL NUMBER OF PAGES: The total page count should follow normal pagination procedures, i.e., enter the number of pages containing information.

7b. NUMBER OF REFERENCES: Enter the total number of references cited in the report.

8a. CONTRACT OR GRANT NUMBER: If appropriate, enter the applicable number of the contract or grant under which the report was written.

8b, 8c, & 8d. PROJECT NUMBER: Enter the appropriate military department identification, such as project number, subproject number, system numbers, task number, etc.

9a. ORIGINATOR'S REPORT NUMBER(S): Enter the official report number by which the document will be identified and controlled by the originating activity. This number must be unique to this report.

9b. OTHER REPORT NUMBER(S): If the report has been assigned any other report numbers *(either by the originator or by the sponsor)*, also enter this number(s).

10. AVAILABILITY/LIMITATION NOTICES: Enter any limitations on further dissemination of the report, other than those imposed by security classification, using standard statements such as:

(1) "Qualified requesters may obtain copies of this report from DDC."

(2) "Foreign announcement and dissemination of this report by DDC is not authorized."

(3) "U. S. Government agencies may obtain copies of this report directly from DDC. Other qualified DDC users shall request through _____."

(4) "U. S. military agencies may obtain copies of this report directly from DDC. Other qualified users shall request through _____."

(5) "All distribution of this report is controlled. Qualified DDC users shall request through _____."

If the report has been furnished to the Office of Technical Services, Department of Commerce, for sale to the public, indicate this fact and enter the price, if known.

11. SUPPLEMENTARY NOTES: Use for additional explanatory notes.

12. SPONSORING MILITARY ACTIVITY: Enter the name of the departmental project office or laboratory sponsoring *(paying for)* the research and development. Include address.

13. ABSTRACT: Enter an abstract giving a brief and factual summary of the document indicative of the report, even though it may also appear elsewhere in the body of the technical report. If additional space is required, a continuation sheet shall be attached.

It is highly desirable that the abstract of classified reports be unclassified. Each paragraph of the abstract shall end with an indication of the military security classification of the information in the paragraph, represented as *(TS)*, *(S)*, *(C)*, or *(U)*.

There is no limitation on the length of the abstract. However, the suggested length is from 150 to 225 words.

14. KEY WORDS: Key words are technically meaningful terms or short phrases that characterize a report and may be used as index entries for cataloging the report. Key words must be selected so that no security classification is required. Identifiers, such as equipment model designation, trade name, military project code name, geographic location, may be used as key words but will be followed by an indication of technical context. The assignment of links, roles, and weights is optional.

Effects of Particulate Matter on Atmospheric Propagation of CO_2 Laser Radiation

D. C. Smith
R. T. Brown
F. G. Gebhardt
P. J. Berger

United Aircraft Research Laboratories
East Hartford, Connecticut 06108

July 1973

SUMMARY

The influence of aerosols, or particulates, on thermal blooming and gas breakdown of 10.6 micron wavelength radiation has been measured. When particles are irradiated with high intensity pulsed CO_2 laser beams, gas breakdown is initiated and the plasma formed limits the propagation of the beam. Experimental measurements of the threshold for ionization of single particles electrodynamically suspended at the focus of a beam have been measured. For alumina particles the threshold was independent of particle size from 1 to 70 micron diameter and was 0.4 - 1 x 10^8 W/cm^2. The threshold was found to decrease with increasing background pressure, apparently the result of retardation of the particle vapor expansion. Streak photographs of the plasma expansion and schlieren studies are also reported. A theoretical analysis of solid particles laser radiation interaction indicates that the mechanism leading to breakdown is superheating of the particle material with subsequent ionization of the solid or of the material directly adjacent to the solid. Experiments were carried out to examine the thermal blooming of a cw CO_2 laser beam propagating in a carbon dust ladened gas used to simulate aerosols and this blooming was compared with that caused by a molecular absorber. Measurements were also made of the time required to heat single electrodynamically suspended particles to incandecence in a cw CO_2 laser beam; this time is a measure of the rate of energy absorption. Transient thermal blooming of a pulsed CO_2 laser beam was examined in the time regime where the laser pulse was comparable to the acoustic transit time across the beam, τ_a. The results show the advantage of reduced thermal distortion for laser pulses whose duration is short compared to τ_a.

TABLE OF CONTENTS

CHAPTER 1

INTRODUCTION

The two main non-linear propagation problems associated with high power laser radiation in the atmosphere are thermal blooming and gas breakdown. These two effects can occur in clean air but they can be an even more severe limitation if atmospheric aerosols or particulate matter are present. The subject of this report is the influence of particles on the non-linear propagation of high power laser radiation.

Gas breakdown is the ionization of air by the interaction of high power laser radiation with the gas and is generally associated with pulsed laser sources. When breakdown occurs the plasma produced attenuates the laser radiation and shields the intended target. For laser pulses that are longer than 10^{-7} seconds the threshold at 10.6 micron wavelength for clean atmospheric air is predicted to be 3×10^9 W/cm^2 (Refs. 1, 2). If sufficient care is taken to filter the air and reduce the dust amounts to a low level this is the observed value (Refs. 3, 4). However if atmospheric aerosols are present the threshold can be several orders of magnitude lower than the clean air value. During the present contract, experimental and theoretical investigations of the breakdown threshold in the presence of particulate matter have been carried out. A unique aspect of this study was the use of an electrodynamic suspension apparatus which allowed the study of a single particle interaction with the laser radiation. The particle of known size and material, was suspended at the focus of a pulsed CO_2 laser and the threshold for ionization of the air was studied as a function of particle material, size, background air pressure, laser spot size and laser pulse duration. The results of these experiments are presented in the next chapter as well as a theoretical model which aids in interpreting the data. In addition to the threshold measurements, diagnostic measurement of the laser plasma expansion time history were made and schlieren photographs of the shock wave were taken.

Thermal blooming, or self-induced thermal distortion, is the degradation of the laser beam caused by the thermal lens formed in the atmospheric path by the energy absorbed from the laser beam (Refs. 5, 6). The energy absorbed is normally associated with that due to molecular transitions or the absorption by rotational transitions of water vapor. The time required to transfer that absorbed energy into heating, of the gas is generally fast and can be considered instantaneous. (This is not true in the case of kinetic cooling which in dry air can occur for times of the order of milliseconds.) Another source of absorption is that due to aerosols or particles present in the air. The aerosol contribution to absorption and subsequent heating is particularly important in the

3 to 5μ atmospheric window. It has been found that molecular absorption of atmospheric constituents for some selected laser lines of DF is extremely low (of the order 10^{-8} cm^{-1}) and is potentially very attractive for atmospheric propagation because of the reduction in thermal blooming (Ref. 7). However if the aerosol absorption leads to heating of the air path, this would also cause blooming and would make the DF laser less attractive. The amount of absorption and relative merit of the different/ASPRS would depend on atmospheric conditions of aerosol concentration and other absorbing constituents in order to compare the different laser sources. Experiments have been carried out on a laboratory scale to compare the thermal blooming which results from particle heating to that caused by molecular absorption. An aerosol cloud was introduced into a cell and the thermal distortion of a CO_2 beam passing through this cell was measured. The particle density and size distribution was measured as well as the transient response of the laser beam to the thermal distortion. In addition, single carbon particles were suspended at the focus of a cw CO_2 laser and the time required for the particles to heat to incandescence was measured.

In Chapter 4, the transient thermal blooming problem is examined. The analysis and potential advantage of using laser pulses whose duration is short compared to the acoustic transient time across the laser beam, τ_a, were discussed in Ref. (8). Briefly, the formation of the thermal lens requires that the density gradients have sufficient time to establish the self-induced lens; this requires a time on the order of the, τ_a. Experiments were carried out using a specifically designed pulsed CO_2 laser whose pulse duration was ~ 3 μsec. The relative advantage of a pulse short compared to, τ_a, was demonstrated experimentally by propagating the laser pulse in a high pressure cell seeded with absorbing gas with nitrogen and also with helium as the background gas. The change in background gas allowed a comparison of propagation under conditions of variable τ_a.

CHAPTER 2

PARTICLE INDUCED GAS BREAKDOWN

2.1 Theory of Particle Induced Gas Breakdown

As mentioned previously, particulates have various effects on a propagating 10.6μ laser beam, ranging from particle-induced thermal blooming in moderate intensity cw beams up to particle-induced gas breakdown in high-intensity pulsed beams. The present analysis deals with the problem of particle-induced gas breakdown in pulsed beams. Experimental evidence indicates that particulates can significantly lower the breakdown threshold of air, and that particulates may account for the dependence of the breakdown threshold on the laser spot size.

As outlined in (Ref. 8), in order to understand the effects of particulate matter on the breakdown threshold, it is necessary to investigate three phases in the laser-particle interaction: (1) the laser energy absorption process at the surface of the particle or in the particle volume, (2) the particle vaporization kinetics, and (3) the interaction of the vapor with the ambient air.

The absorption of radiation by a particle (Ref. 9) depends on the complex index of refraction of the particle at the wavelength of interest ($n = n_1 - in_2$) and, for a spherical particle, on the quantity $x = 2\pi a/\lambda$, where a is the particle radius and λ is the wavelength. The energy absorption cross section is equal to $\pi a^2 Q_{abs}$, where Q_{abs} is the efficiency factor for absorption. For particles such as carbon ($n_1 = 1.95$, $n_2 = 0.66$), Q_{abs} varies from being nearly proportional to a (i.e., volumetric absorption) at small values of x, to being independent of x (i.e., optically thick absorption) for large values of x ($Q_{abs} \approx$ for $x \gtrsim 1$ for carbon).

Thus, we would expect that at $\lambda = 10.6\mu$, the absorption process at the surface of particles of ~10μ diameter or larger would be similar to the absorption process at a solid surface. In (Ref. 8), the results of previous studies of laser-surface interactions were summarized and curves, based on the work of Chang, et al, (Ref. 11) were presented showing the vapor velocity, vapor density and vapor temperature vs. the laser intensity for 10.6μ radiation and an infinite quartz surface in vacuum. If one assumes that the ambient air has a negligible effect on the expanding vapor, one can then estimate the shock strength in air corresponding to the vapor velocity so obtained. As indicated in (Ref. 8), the results for quartz, at intensities over the range 10^6 - 10^8 W/cm^2, lead to shock heated air temperatures as high as ~ 5000°K, with corresponding ionization fractions (n_e/n) of 10^{-4}.

While this level of ionization is probably sufficient to initiate gas breakdown via cascade ionization, the shock heating process appears to have one feature which is not consistent with experiment. In (Ref. 8), it was shown that the vapor expansion velocity and hence the vapor driven shock strength are relatively weak functions of the incident intensity. On the other hand, as mentioned in (Ref. 8), the experiments with 50μ particles show a very sharp threshold for breakdown. Thus, based on the above arguments, it would appear that the breakdown threshold for optically thick particles is determined by heating and ionization of the particle material rather than vapor-driven shock heating of the ambient air.

Since the majority of the particles in a typical aerosol laden atmosphere are less than 10μ in diameter (Ref. 8), a second analysis has been carried out in an attempt to understand the heating and vaporization processes for optically thin particles. Initially, calculations were carried out for a Sedov-type model similar to that used by Nielsen and Canavan (Ref. 10). For these initial calculations, the particle was assumed to vaporize in place at the vaporization temperature T_o, defined as the temperature at which the vapor pressure was equal to the ambient gas pressure (typically 1 atm). It was assumed that the vapor expanded with uniform temperature and pressure and with a velocity that varied linearly from the center to the outer edge of the vapor sphere* according to the equations

$$\frac{4}{3}\pi\rho r^3 = M = \text{const} , \tag{1}$$

and

$$\rho 4\pi r^2 \frac{dr}{dt} = \frac{1}{2}\left(\frac{3}{5}M\right)\frac{d}{dt}v^2 , \tag{2}$$

$$\frac{3}{2}nk\frac{dT}{dt} = -4\pi pr^2 v + W , \tag{3}$$

where ρ is the vapor density, r is the coordinate of the outer edge of the vapor sphere, M in the total vapor mass, p is the pressure, v is the velocity at the outer edge of the vapor shell, N is the total number of vapor particles, T is the temperature, and W is the rate of energy input to the vapor from the laser. The vapor was treated as an ideal gas with the equation of state

$$p = \frac{3NkT}{4\pi r^3} \tag{4}$$

---

* The results of Nielsen and Canavan for the same initial conditions, but using a hydrodynamic code showed that for the optically thin case, the Sedov model is good approximation to the hydrodynamic model.

and the energy input term had the form

$$W = \mu M I_o \ , \tag{5}$$

where μ is the mass absorption coefficient and I_o is the incident laser intensity. The mass absorption coefficient was assumed to have the form

$$\mu = \mu_o \ (\rho/\rho_o)^{n-1} \tag{6}$$

where μ_o is the mass absorption coefficient of the solid, and n = 2 is a typical value based on the theory of pressure broadening applied to quartz vapor (Ref. 11).

These equations can be written very simply in terms of the dimensionless variables $x = r/r_o$, where r_o is the radius of the particle, $z = T/T_o$, $v_o = (5k\ T_o/\overline{m}\ )^{\frac{1}{2}}$, where $\overline{m}$ is the average mass of a vapor molecule, $y = v/v_o$, and $w = tv_o/r_o$ as

$$\frac{dx}{dw} = y \ , \tag{7}$$

$$\frac{dy}{dw} = \frac{z}{x} \ , \tag{8}$$

$$\frac{dz}{dw} = - \frac{2zy}{x} + G_1 \left(\frac{1}{x}\right)^{3n-3} \ , \tag{9}$$

$$G_1 = \frac{2}{3} \ \overline{m} \ \frac{I_o \mu_o}{K} \ \frac{r_o}{v_o T_o} \tag{10}$$

is a parameter which, for a given particle material and size, is proportional to the incident laser intensity. The equations have the initial conditions x (o) = 1, y (o) = 0, and z (o) = 1, and, when integrated, reach a quasi-steady solution in which z reaches a maximum and then decays asymptotically to zero and y asymptotically reaches a steady state value y_∞ on a time scale $w \approx 1$.

Plots of z_{max} and y_∞ vs G_1 are shown in Fig. 1. For values of G_1 less than 1, the vapor starts at the temperature T_o and a density equal to the solid density* and reaches the velocity v_o, with no further heating. At higher values of G_1, for which vapor heating is important, the vapor reaches a peak temperature greater than T_o and a velocity greater than v_o.

For a spherical particle, the parameter G_1 can be re-written in terms of the absorption efficiency factor mentioned previously as

$$G_1 = \frac{Q_{abs}}{2} \frac{I_o}{n_o k T_o v_o} \tag{11}$$

Taking $Q_{abs} = 1$(the largest value for which an optically thin analysis would apply), and using the properties of quartz, gives $G_1 = 0.4$ for $I_o = 1.0 \times 10^8$ W/cm^2.

These results can be used to estimate the strength of a vapor driven shock wave in a manner similar to that for the optically thick case outlined in (Ref. 8). For the case of quartz described above, one obtains a shock Mach number in air of 5 (based on plane shock relations). This value is somewhat low for shock heating of air; however, the major conclusion to be drawn from Fig. 1 is that the vapor expansion velocity is only weakly sensitive to the incident intensity, particularly at the low values of G_1 corresponding to the experimentally measured values of aerosol-induced air breakdown. This fact, coupled with the fact that strong shock heating, based on the theory, would require much higher intensities than those measured experimentally, indicates that the Sedov model described above is not capable of explaining the aerosol-induced breakdown data.

In an attempt to obtain a better model of the vaporization process, the above formulation was extended to include the vaporization kinetics of the particle and to start with self consistent initial conditions.** The solid was assumed to absorb the laser energy uniformly (i.e., the particle was taken to be optically thin as before) and to vaporize from its surface at a rate given by

$$\dot{M}_v = A_s \left(\frac{\overline{m}}{2kT_s}\right)^{1/2} p_v \quad , \tag{12}$$

---

* Note that this implies on initial pressure in the vapor of the order 10^4 atm.

** The previous model ignored the vaporization kinetics, and instead started with the somewhat arbitrary initial condition of a fully vaporized particle at solid density.

where A_s is the surface area of the solid particle, T_s is the temperature of the particle, and p_v is the vapor pressure at the temperature T_s.

The solid particle was assumed to conduct energy to the vapor (taken to be uniform in temperature) via an effective conduction term, written

$$W_c = \frac{k_v A_s (T_s - T_v)}{\bar{r}} \quad , \tag{13}$$

where W_c is the rate of energy conduction k_v is the thermal conductivity of the vapor, T_v is the vapor temperature, and $\bar{r}$ is an effective conduction length to account for the spherical geometry ($\bar{r} \sim 0.1\ r$ typically).

The governing equations can then be non-dimensionalized as before, and the equations for x and y written as in Eqs. (7 and 8) above. The equations for the vapor temperature ($z_v = T_v/T_o$), the vapor fraction ($x = M_v/M$), and the solid particle temperature ($z_s = T_s/T_o$) can be written symbolically as

$$\frac{dz_v}{dw} = V_1 + V_2 - V_3 \quad , \tag{14}$$

where V_1 is the energy transferred to the vapor via conduction, and V_2 and V_3 are the vapor absorption and expansion energy terms appearing in Eq. (9),

$$\frac{dx}{dw} = A \quad ,$$

where A is the non-dimensionalized form of the vapor production term in Eq. (11), and

$$\frac{dz_s}{dw} = G_1 - S_1 - S_2 \quad , \tag{15}$$

where S_1 is the energy lost from the solid due to vaporization and S_2 is the energy lost from the solid via thermal conduction.

Typical solutions for conditions corresponding to a 10μ diam quartz particle with an incident flux of 5×10^8 W/cm^2 are shown in Fig. 2. For these conditions, w = 1 corresponds to t = 3 nsec. From Fig. 2 it can be seen that when the vapor begins to expand, the vapor temperature tends to drop (at this intensity, vapor absorption is negligible), whereas the solid temperature continues to rise to a rather high superheated value.

Data analogous to those in Fig. 1, but based on the modified Sedov model described above, are shown in Fig. 3. At the lower values of intensity (i.e., of G_1),

superheating of the solid is the dominant heating mechanism, whereas, at high values of intensity, vapor absorption and heating dominate.

Similar results, but for conditions corresponding to a carbon particle, are shown in Fig. 4. Because of the slower vaporization rate for carbon, compared to quartz, the superheating is much more pronounced, and the solid reaches very high temperatures even for relatively low intensities.

The general conclusions to be drawn from Figs. (1-4) are as follows:

1) For the laser intensities corresponding to the experimentally measured aerosol laden air breakdown thresholds, the vapor expansion velocity is not high enough to cause shock heated air ionization and is therefore not the likely explanation of the low threshold.

2) For these same intensities, laser energy absorption in the vapor is too low to significantly heat the vapor, and thus, direct ionization of the vapor is not the likely cause of breakdown.

3) It appears that the most likely cause of breakdown (for the short laser pulses being considered in this study) is superheating of the particle material, due to the finite vaporization kinetics, with subsequent ionization of the solid or of the material directly adjacent to the solid.

2.2 Particle - Induced Gas Breakdown - Experimental

The experimental studies of particle induced breakdown during the final phases of this contract were concerned with determining the dependence of the breakdown threshold on particle size, laser spot size, and background gas pressure. In addition diagnostic measurements of the plasma expansion velocity using streak photography as well as schlieren photography have been carried out.

A brief review of the previous data will be given; the details are contained in Ref. (8). During the first six months of the contract, the experimental investigations involved the setting up of the particle suspension apparatus, and investigating the threshold for vaporization and ionization as a function of particle material and pulse duration. The particle suspension apparatus consisted of a cubical array of six electrodes with each pair of opposite electrodes connected to one phase of a three-phase ac supply with a variable voltage of up to 3 Kv. Particles were dropped through a high voltage discharge, picking up sufficient charge so to be captured in the AC field. DC bias was applied to each pair of electrodes in order to position the particle at the focus of a germanium lens. This technique allows single particle-laser radiation interaction studies where the size and particle material can be made experimental variables. The laser used in these studies was an electrically pulsed TEA configuration CO_2 laser with an output of approximately one joule with a 0.2 μsec leading spike and a 2 μsec lower intensity tail. The laser could be operated without nitrogen producing a well defined pulse of 0.2 μsec full width at half maximum and no tail. This pulse was used in the majority of the experiments because the pulse was more well defined. The studies showed that the threshold for plasma production depends on the peak intensity of the pulse and not the energy flux for laser pulses of 0.2 to 2 μsec duration. The threshold was independent of particle material for wide variety of materials including salt, carbon, clay, germanium, aluminum and silica. The threshold value was in the range of $1 - 2 \times 10^8$ watts/cm^2. When a breakdown occured, the plasma produced attenuated subsequent portions of the laser pulses. The time required for the plasma to expand and fill the laser spot was consistent with that calculated for a laser supported blast wave. At intensities below threshold, some of the particles could be shattered or vaporized, and this threshold for particle elimination was found to be dependent not on the peak intensity but rather on the energy flux contained in the pulse. The threshold for eliminating the particles ranged from 5 joules cm^{-2} for carbon and clay to 50 joules/cm^2 for germanium; salt particles did not interact with the laser radiation without breaking down, i.e., the salt could not be eliminated without plasma production. During the first part of the contract only particles of 50 μ diameter were used; during this report period the diameter dependence of the threshold was examined and reported below.

Particle Size Dependence

The particle size dependence of the threshold was examined using alumina particles (Al_2O_3). The size range was from 1 to 70 microns diameter and the threshold data is shown in Fig. 5. The number next to the data refer to the number of breakdowns observed out of ten shots. The threshold appears to be independent of particle size for the material and size range. This is somewhat surprising in view of previously reported results by the Lincoln Laboratory (Ref. 14) which showed a size dependence for particles smaller than 10 μmicrons. This dependency has not been resolved.

The particle sizes were determined by micro photographing a slide containing a sample of the particles. The large size particles were spherical in shape and were within 10 percent of the specified size. The smaller particles, (≤ 8 microns) were irregular in shape and some variation in size was observed. The one micron size particles had a tendency to adhere together and form clusters which could affect the measurement of the threshold. From the microscopic photos it appears that the one μ micron particles formed clusters of two or three particles. This probably would not have a significant effect on the breakdown threshold since the bonding must be weak and the laser interaction would break the bond at a low laser beam intensity and therefore the interaction of the high intensity beam would be between the small particle and the laser radiation rather than with the cluster of particles.

Laser Spot Size Dependence

The laser spot size in the previous experiments was fixed at 500 microns diameter. Since the laser interaction involves an expanding vapor it was felt important to determine if the threshold depended on the relative size of the particle compared to the laser spot size. The focal spot size was varied by using different focal length lenses for the small spot diameters and spherical mirror were used to produce the largest spots.

The data for the breakdown threshold intensity of the various alumina particles as a function of laser beam diameter are shown in Figs. 6-9. Each Fig. shows data for a fixed sized particle from 3 micron up to 50 micron diameter. The laser spot size was varied over the range from 2.5×10^{-2} cm up to a maximum diameter of 0.15 cm. The data shows some scatter with the threshold varying from 2 to 5×10^7 watts/cm^2. No systematic trend in the data is observed and it is concluded that the breakdown threshold is independent of the laser beam diameter for these experimental conditions.

It should be noted that earlier preliminary data had shown an apparent laser spot size dependence and this data was presented at an ARPA/STO meeting held at Mitre Corporation in June 1973. This data was found to be in error. The apparent diameter dependence was caused by deflection of the beam by the germanium attenuator. For small beams the deflection of the beam by the wedged attenuator shifted the beam and therefore showed an apparent higher threshold. For the data shown in Figs. 6 through 9, the deflection of the beam was accounted for by realigning the

beam on a wire located at the telescope cross-hairs when each attenuator was inserted in the beam. The error introduced was greatest for the small beam diameters ($\leq 10^{-2}$cm) and little error was introduced for laser beams of 500 microns diameter which was used in the previous experiments on material dependence. For future experiments, a better technique for attenuating the beam should be determined; perhaps germanium flats with no wedge would eliminate the tedious job of realignment of the beam for each attenuator.

Background Gas Pressure

The gas breakdown threshold of laboratory air had shown a pressure dependence. This threshold was controlled by the presence of aerosols but the pressure dependence was not well understood. The pressure dependence could be related to the probability of finding an aerosol in the laser beam or could be associated with the dynamics of the interaction of the expanding particle vapor with the laser radiation. By studying the pressure dependence of the threshold of a single solid particle the mechanism can be identified.

A pressure tight suspension cell was built for these tests. It was found that the pressure could only be lowered to 170 torr because of electrical breakdown between the suspension electrode at lower pressure. It also was not possible to charge the particles at low pressures and so it was necessary to suspend the particles at atmospheric pressure and then reduce the pressure by slowly evacuating the chamber. The pressure dependence of the threshold of aluminum and carbon particles as a function of background air pressure is shown in Fig. 10. The aluminum particle breakdown has a slight pressure dependence on background pressure while the carbon has a somewhat stronger pressure dependence. This pressure dependence is consistant with that observed for laboratory air. The conclusion reached is that the background pressure retards the vapor expansion and leads to a lower breakdown threshold.

Particle Plasma Expansion

The expansion of particle induced breakdown plasma is of interest both in aiding in determining the mechanism causing the plasma production and also to examine the rate at which the laser beam is extinguished by the expanding plasma. An STL image convector camera was used to examine the particle plasma expansion. The camera was used in the streak mode to examine the expansion. Two types of particles were examined, both salt and aluminum and for comparison, a 250 micron diameter wire.

The streak photograph for a 50 micron diameter aluminum particle is shown in Fig. 11. A sketch of the lens and position of the focus is shown at the top and the streak photograph of the plasma luminosity growing toward the focusing lens. The initial position of the particle is also shown in the photograph. The lower photograph is an oscilloscope trace which shows the laser pulse (upper trace)

and the ramping voltage pulse of the STL streak unit (lower trace) and shows the relationship of the laser intensity and the streak photograph. As closely as can be measured the plasma luminosity is first recorded at the peak of the laser pulse and the expansion velocity is 7×10^5 cm/sec. A streak photograph of the plasma produced off of the surface of a 250 micron diameter wire is shown in Fig. 12. The plasma appears to be formed earlier in the pulse but has the same initial expansion velocity. This velocity increases with time when the laser pulse reaches its peak value. Longer duration streak photos were also taken to determine the plasma lifetime. Fig. 13 is a long duration streak photo which shows that the plasma luminosity lasts for times on the order of 5 μsec. A streak photograph of a 50 μmicron diameter salt particle is shown in Fig. 14. Qualitatively, the expansion velocity and plasma lifetime for the salt is the same as that observed for the aluminum particle.

Schlieren Studies

As discussed in Ref. 8, extensive measurements have been made of the vaporization and breakdown threshold of a single particle using the output pulse from a CO_2 TEA laser. During the second half of the contract period, schlieren photographs were taken of the vaporization and breakdown processes in order to gain further insight into the basic mechanisms controlling the threshold.

A diagram of the experimental apparatus is shown in Fig. 15. The spark source emitted a light pulse with a 50 nsec halfwidth allowing the observation of high Mach number shock waves in air, and the viewing optics provided a 20 x magnification, allowing the observation of particles down to 5 μ in diameter. Because of spatial and temporal resolution limitations, the system was not intended for use during the laser pulse; i.e., attempts were not made to photograph the particle during the time in which it was actually being irradiated by the laser pulse. Instead the system was used primarily to study the following two questions: 1) Whether the particle could be vaporized sufficiently to generate a shock wave in air, without causing actual breakdown and 2) whether the particle was vaporized first and then ionized, causing breakdown; or was only partially vaporized when breakdown occured.

A typical set of schlieren photographs is shown in Fig. 16. In these pictures, the laser pulse consisted of a 200 nsec halfwidth spike with no tail, and the schlieren spark source was fired 500 nsec after the peak of the laser pulse. The particles were 50 μ diameter carbon suspended in STP air and the laser focal diameter was 650 μ. The first picture shows that a vapor-driven shock wave was generated at the particle at a flux below that required for breakdown. The second photograph corresponds to an intensity very close to threshold. It should be noted that the luminosity due to the breakdown plasma is time integrated (there was no shutter on the schlieren camera) whereas the shock image corresponds to a given instant of time. The striations in the breakdown plasma may be due to self mode locking of the TEA laser. The final photograph in Fig. 16 is for an intensity well above

threshold and clearly shows that the breakdown was initiated at the front surface of the particle, leaving the particle more or less in tact. It appears that the breakdown region expanded to fill the laser focal volume, and then propagated back toward the laser.

All of the data taken in this series of tests were for the optically thick case (i.e., $x = 2 \pi a / \lambda > 1$) and as expected, the results indicate that breakdown occurs at the front surface of the particle. While insufficient tests were carried out to determine whether shock heating of the air or direct surface heating initiated breakdown one can conclude that breakdown occurs prior to complete vaporization of the particle.

2.3 Summary and Conclusions

Results have been presented regarding the initiation of gas breakdown by a single particle suspended in air. Approximate theoretical models have been presented (in this report and in Ref. 8) for the two cases of optically thick and optically thin particles. Experimental results have been presented concerning the effects of particle material, particle size, laser spot size, and background gas pressure on the thresholds for vaporization and for particle initiated gas breakdown. The results of these studies can be summarized briefly as follows:

Theoretical

1) The theoretical study for optically thick particles, based on the results of Chang, et al (Ref. 11) for quartz and extended approximately to the case of vapor expandion into a background gas and subsequent shock heating of the gas yields an ionization fraction of 10^{-4} at intensities in the range 10^6 - 10^8 W/cm^2. This value of electron density could lead to gas breakdown. However, the results show only a weak dependence on the incident intensity, and consequently do not provide a good explanation of the experimental data. It is possible that a more rigorous treatment of the vapor-gas interaction would resolve this question, however, such an analysis is beyond the scope of the present study.

2) The theoretical study for optically thin particles, based on a modified Sedov model, indicate that vapor-induced shock heating requires very high intensities ($> 10^9$ W/cm^2) to produce ionization fractions of 10^{-4}, and again shows a weak dependence on the intensity. Therefore, for optically thin particles, the most likely cause of the low threshold is direct surface heating.

Experimental

1) The threshold for vaporization/shattering of the particle (i.e., no breakdown) depends on the energy flux of the pulse, rather than on the intensity.

2) The threshold for breakdown, i.e., ionization depends on the peak intensity of the laser pulse.

3) The breakdown is initiated at or very near the surface of the particle and expands to fill the laser focal volume on a 10-30 nsec time scale. From then on, the plasma propagates toward the laser as a laser-supported blast wave.

4) The breakdown threshold is independent of particle size, for particles in the 1-70 μ range. For particles of 3 μ diameter or greater (i.e., $x = 2\pi a/\lambda > 1$), this is not too surprising, since these particles would all tend to be optically thick, and the laser-solid interaction would tend to be similar to that at an infinite surface. However, based on theoretical considerations, one would expect the one micron particles to have a higher threshold. This discrepancy is presently unexplained.

5) The threshold for vaporization/shattering was dependent on particle material; however, the breakdown threshold was almost independent of particle material and was in the range $1 - 2 \times 10^8$ W/cm^2 for most particles studied and was lowest for alumina at a 0.4×10^8 W/cm^2.

6) The breakdown threshold appears to be independent of the laser spot size for particles in the 3 to 50 micron diameter range and laser spot diameter in the 2.5×10^{-2} cm to 0.15 cm range. This is consistent with a breakdown mechanism in which the laser-particle interaction is predominantly a surface effect and occurs on a dimension small compared to the laser spot size.

7) There appears to be a slight dependence of the breakdown threshold on the background gas pressure similar to that for laboratory air breakdown. This behavior is probably related to the vapor-gas interaction, but, as mentioned above, is beyond the scope of the present analysis, and has not been explained theoretically.

CHAPTER 3

CW LASER-AEROSOL INTERACTIONS

3.1 Incandescense of Carbon Particles with cw CO_2 Laser Radiation

In order to gain a better understanding of the absorption of laser radiation by particulates, and to study the transfer of this energy to the surrounding air, experiments have been carried out with single carbon particles suspended in air at the focus of a cw CO_2 laser. The experimental setup for these measurements was the same as that for the pulsed studies as shown in Fig. 15 with the exception that a 10 W cw laser was substituted for the TEA laser. The particles were suspended electrodynamically as before and the laser radiation was switched on with a high speed shutter ($\sim$ 3 msec risetime). In these experiments, the Schlieren spark was fired at various delay times, τ_d, with respect to the opening of the shutter. Typical results are shown in Figs. 17 and 18. As with the pulsed-laser photos, there was no shutter on the Schlieren camera, so that the bright flash observed at the focus of the laser was integrated in time, whereas the Schlieren field and the corresponding dark image of the particle occured at a single instant in time. From the sequence in Fig. 17 it can be seen that the particle reached incandescence and was very quickly knocked out of the suspension cube. In each picture in the sequence (with a new particle on each shot), a bright flash was observed visually at the time the 10.6μ shutter was opened. In Fig. 18, a 100μ particle is shown before being irradiated and is shown again 20 msec after the shutter was opened. Since the particle has moved out of the incandescent region at the time of the schlieren photo, this picture clearly shows that the particle reached incandescence on a time scale less than 20 msec. The general conclusions from these and other similar pictures are as follows: 1) Carbon particles of 50μ diameter or greater, in STP air, heat to incandescence at a flux of 3×10^3 W/cm^2, 2) This heating occurs in time on the order of 10 msec. 3) The particles do not reach the vaporization temperature (particles outside of the incandescent region do not appear to have lost any mass), 4) The 100μ particles reached a higher temperature than the 50μ particles (as expected based on the energy absorption, and thermal conduction processes).

3.2 cw Thermal Blooming Caused by Aerosol Heating

Under typical atmospheric conditions, the absorption of 10.6μ radiation by various molecular species results in an absorption coefficient of approximately 1.5×10^{-6} cm^{-1}, and leads to various non-linear propagation problems (Ref. 12).

For some lasers the molecular absorption in the air is small ($< 10^{-6}$ cm^{-1}) and the heating due to aerosols can dominate the heating of the air path. For a typical atmosphere, this aerosol absorption corresponds to an attenuation coefficient of approximately 10^{-7} cm^{-1}, but could be higher if the aerosol concentration were unusually high (Refs. 13, 15). In general, it is not the linear loss in power which is important but rather the non-linear effects which result from the heating.

The heating of air due to particulate absorption differs from that due to molecular absorption in that the heating occurs at discrete centers in the gas, and for typical aerosol concentrations (5000 particles/cm^3) these centers are quite widely-spaced. Thus, an important consideration in determining the effect of aerosol heating on the laser propagation is the time evolution of the temperature profile. A typical set of profiles, for the case in which the intensity is turned on at time z = 0 is sketched in Fig. 19. Initially the thermal disturbances are concentrated in regions close to the particles, but after the profiles from individual particles have merged, the average temperature of the gas rises at a rate determined by the heat capacity of the gas and the macroscopic absorption coefficient associated with the particles. The time for the individual profiles to merge can be estimated from the thermal diffusion time associated with the mid-point distance between particles a_p shown in Fig. 19. This time τ_{TD} is given by the relation

$$\tau_{TD} = \frac{a_p^2 \rho c_p}{4 k} \qquad (16)$$

where ρ, c_p and k are the density, specific heat and thermal conductivity of the gas, and, for air at STP and a particle concentration $n_p = 5000$ cm^{-3}, has the value $\tau_{TD} \approx 1$ msec.* Since for many cases of interest this is shorter than the other pertinent times (e.g., the transit time across the beam for the case of thermal blooming in the presence of a wind), we would expect the thermal blooming effects due to aerosols to be similar to those for molecular absorbers.

In order to obtain a direct measure of the beam distortion due to a particulate laden atmosphere, experiments were carried out in a cell containing air and fine carbon dust. The carbon particles were introduced through a small hole in the side of the cell and were blown into suspension using a swirling air jet. A portion of the experimental arrangement is shown in Fig. 20. In the

*This expression applies to a collection of particles of the same size (i.e., with the same absorption cross section). For an aerosol with a distribution of particle sizes, an effective thermal diffusion time could be estimated by taking a weighted average over the particle size distribution and the corresponding absorption cross section.

upper photograph, the He-Ne beam (which is co-linear with the CO_2 beam) can be seen as scattered light from the particles in the cell. The lower photo shows a closeup of the particles in the He-Ne beam (the bright spots at the left in the picture are reflections from the beam splitter and NaCl window faces). In the experiments, the beam distortion varied slowly with time as the particles settled out in the cell, with the attenuation over the 1.5 m cell length varying from $\sim$ 90% immediately following suspension of the particles to $\sim$ 0% approximately two minutes later. This allowed measurement of the beam distortion for various particulate concentrations. The present experiments were carried out with no transverse wind, and consequently show the effects of particulate induced blooming in the presence of natural convection.

Typical photographs of the beam profile with various degrees of distortion are shown in Fig. 21. The profiles are qualitatively similar to those observed with molecular absorption. The second photograph in Fig. 21 corresponds to a linear attenuation of $\sim$ 35%.

Quantitative measurements of the particle-induced beam distortion were made using an integrated irradiance analyzer, which measured the integrated power out to a radius r in the beam, as a function of the radius r. Typical results are shown in Fig. 22. Data for molecular absorption with conditions chosen to give nearly the same overall beam attenuation for the particles and for the moleculars, are shown for comparison. It can be seen that in both cases, the centerline intensity is reduced by approximately a factor of four, whereas the total power is only reduced $\sim$ 30%, indicating a fairly strong non-linear distortion effect. In these measurements, part of the particulate attenuation was due to scattering (see discussion below) rather than solely to absorption, as with moleculars, and this is reflected in the smaller amount of distortion for carbon particles versus that for CO_2 shown in Fig. 22.

In order to measure the time response of the particle induced blooming, the centerline beam intensity was measured with a point detector, with the beam switched on at time t = 0. Typical results are shown in Fig. 23. The intensity rises initially to its undistorted value and then begins to drop as energy is transferred from the particles to the gas, causing thermal lensing. This process stops when natural convection establishes a steady state energy balance in and out of the beam. The response times of the shutter and detector system ($\sim$ 50 msec) were not fast enough to examine the inter-particle temperature profile evolution effect described above, but the measurements do show that the effects with particulates are qualitatively similar to those obtained with pure molecular absorption.

The particle concentration and size distribution at a given instant of time were determined by drawing a small sample of the particulate laden air through a 0.1μ millipore filter and photographing the particles through a microscope.

A typical photo, corresponding to a total particle density n_p of 10^4 cm^{-3} is shown in Fig. 24. By counting particles in various size ranges, the particle size distribution shown in Fig. 24 was obtained.

In order to measure the fraction of 10.6μ radiation actually absorbed by the carbon particles versus that scattered, measurements were made of the pressure rise in a sealed off absorption cell. The cell consisted of a 1.5 m long x 3.8 cm ID copper tube with the inner wall painted flat black to absorb any scattered radiation. Since the heat capacity of the copper walls was much greater than the air in the cell, the walls acted as a heat sink for scattered radiation. It can be shown that for times short compared to the thermal diffusion time from the 10.6μ beam along the cell centerline (~ 0.5 cm beam diameter) to the cell wall, the rate of energy absorption in the gas is related to the rate of pressure rise by the equation

$$Q_{abs} = \frac{V\,(dp/dt)}{\gamma - 1} \qquad (17)$$

where V is the cell volume, dp/dt is the slope of the pressure curve at the time the laser shutter is opened, and γ is the ratio of specifc heats for air.

The rate of pressure rise in the cell was measured with a type 1023 Barocel Electronic Manometer with the signal displayed on an oscilloscope, and the laser power values at the entrance and exit of the cell were measured with a CRL laser power meter. Figure 15 shows the relative absorption cross section (normalized to the total extinction cross section) for various values of total attenuation. The data were taken by blowing the particles into suspension and taking measurements at various later times (~ 3 minutes for the entire process). Thus, the data at large attenuations (i.e., earlier in the sequence) are with a higher fraction of large particles (since these particles settle out faster) and hence show a higher fraction of scattering versus absorption. At an attenuation of ~ 35%, corresponding to the data in Fig. 22, approximately 60% of the radiation was absorbed, with the remainder being scattered.

In summary, the absorption cell measurements with particulate laden air have shown that pure particulate absorption does lead to thermal blooming, and that for conditions of the present experiments, this distortion is qualitatively similar to that for molecular absorption.

CHAPTER 4

TRANSIENT THERMAL BLOOMING

4.1 Introduction

One potential advantage of short CO_2 laser pulses as compared to cw, is a reduction in the thermal blooming. In order for distortion to occur, the density of the air path must change which takes some fraction of the acoustic transit time across the beam. For times short compared to the acoustic transit time the thermal distortion will be less and this may offer a solution to the thermal distortion problem. Previous research in this area has already shown that there is an advantage to operating in this time regime. Experiments performed at Lincoln Laboratory[16] showed the decrease in distortion for pulse lengths short compared to the acoustic transit time and the theoretical model of Ulrich[17] predicts a reduction in the blooming. In reference 8 a detailed discussion of the non-dimensional parameter involved in laboratory simulation of the transient blooming were given. These are briefly summarized in the next section. The experimental program was carried out using a modified TEA laser where the modifications produced an output pulse of sufficient duration to perform the experiments and also eliminated the leading spike of intense radiation normally associated with TEA lasers. The experimental data demonstrates the potential advantage of using laser pulses whose duration is short compared to the acoustic transit time across the beam.

4.2 Transient Thermal Blooming Theory

Here, only the perturbation expressions for the on-axis intensity are given to aid in interpreting the experimental data. More detailed discussions of the transient theory are given in Refs. 8, 16, and 17. Simple analytical expressions for the transient bloomed on-axis intensity can be obtained using perturbation theory for pulse lengths t_p that are both short and long compared to the acoustic transit time $t_h = a/c_s$, where a is the 1/e intensity beam radius and c_s is the acoustic velocity. Thus, the bloomed on-axis intensity relative to the undistorted value for a pulsed collimated beam uniform in time is given by

$$I_{REL} = \exp\left\{-N_{s,\ell}\right\} , \qquad (18)$$

where for the short time limit ($t_p \ll t_h$)

$$N_s = \frac{4}{3} c \, (t_p/t_h)^2 \, (t/t_p)^3 , \tag{19}$$

and for the long pulse case ($t_p \gg t_h$)

$$N_\ell = c \, (t/t_p) , \tag{20}$$

and, assuming $\alpha z \ll 1$,

$$c = \frac{2}{\pi} \frac{-n_T \alpha z^2 E_p}{n_o \rho_o c_p a^4} . \tag{21}$$

Here, n_o, n_T, ρ_o, c_p and α refer, respectively to the refractive index, the index change with respect to temperature, the density, specific heat at constant pressure and absorption coefficient of the gas, z is the pathlength, a is the 1/e Gaussian beam radius and E_p is the total pulse energy. The relative on-axis intensity is plotted versus time in Fig. 26 for the three cases: $t_p = 0.1\, t_h$, $t_p = t_h$, and $t_p \gg t_h$, with c = 2. The advantage of pulses with regard to reductions in thermal blooming are clearly shown by Fig. 26 to be obtained in the short time limit, where the distortion parameter N_s is reduced by the factor $(t_p/t_h)^2$ below the long pulse value N_ℓ for the same pulse energy. Also, the short and long-time blooming regimes are readily distinguished in Fig. 26 by the t^3 and linear time dependence for N_s and N_ℓ, respectively. Thus, early in the pulse the blooming effects are reduced significantly in the short time limit case as compared with the same pulse energy beam in the long time limit.

To account for focusing, the distortion parameters N_s and N_ℓ in Eqs. 19 and 20 must simply be multiplied by the respective correction factors

$$q_s = \frac{F^4 - 1 + 4 \ln F}{8(1 - 1/F)^2} \tag{22}$$

and

$$q_\ell = \frac{F^2 - 1 + 2\,\ell n\, F}{2(1 - 1/F)^2} \qquad (23)$$

where $F = ka^2/z$ is the Fresnel number with $k = 2\pi/\lambda$ and λ is the wavelength. As the Fresnel number becomes large there is strong focusing of the beam and q_s and q_ℓ reduce, respectively, to $\sim F^4/8$ and $F^2/2$.

4.3 Experimental Arrangement

The laser used in these experiments was a 25-cm long transverse finned-cathode, double-discharge, TEA laser. Three modifications were made to give a long output laser pulse: (1) the circuit parameters in the pulse forming network were chosen to give a long current pulse ($\sim$ 10 μsec); (2) the laser was operated on a nitrogen rich mixture (1:3:8;CO_2:N_2:He); and (3) a relatively high laser output mirror reflectivity of 90% was used, together with a relatively long cavity of 3m, giving small output coupling per pass. The gain-switched spike, more-or-less characteristic of TEA lasers, was not seen. Instead, the laser pulse has a 0.25- μsec rise-time, a full width at half maximum of 0.8 μsec, and an overall duration of approximately 4 μsec. The 3-m long laser cavity is formed by a flat, 100% reflecting copper mirror and a 10-m radius of curvature, 90% reflecting germanium output mirror. Limiting apertures of 1.8 and 2.1-cm diameter are placed adjacent to the mirrors to encourage fundamental mode operation. A pulse energy of 0.16 J is obtained under these conditions. Focusing the output beam with a 1-m focal length mirror gives a focused spot having a $1/e$-beam diameter 0.17 cm. The focus occurs 1.8 m from the face of the mirror due to the curvature of the beam leaving the 10-m radius of curvature output mirror.

The experimental arrangement used to study the transient blooming with these output pulses is shown in Fig. 27. The laser output is focused with the 1-m radius of curvature mirror into a 1-m long gas cell, the focus occuring at the exit window of the cell. Part of the exit beam is deflected by a salt-flat beam splitter into a fast Au:Ge detector, the remainder collected by a power cone used to record the transmitted pulse energy. Part of the input beam is deflected by a salt-flat beam splitter and a turning mirror and travels an equal path length to a reference monitor, a fast Au:Ge detector, allowing pulse-to-pulse differences in the laser output to be recoreded for normalization. Pin hole apertures of 0.08-cm diameter are mounted in front of the sample and reference detectors and centered on the beams to record differences in the on-axis beam intensity. The gas metering system contains the valves and meters required for evacuating ($\sim$ 0.3 torr base pressure) and pressurizing (up to 150 psig) the gas cell. Anti-reflection coated germanium windows could not tolerate the focused intensity at the exit window ($\sim$ 10J/cm^2,

$\sim 10^7$ W/cm^2); and, as a result, 0.9-cm thick polished salt flats of 2-cm diameter are used as cell windows. They withstand the 10-atm pressure differential and the high focused intensity without damage.

For each firing of the laser the transmitted energy is measured and the sample and references traces are taken with a dual beam Tektronix 555 oscilloscope. This information is recorded first with the cell evacuated for normalization purposes. Then, a small amount of SF_6 is added to the cell and diluted with air or helium. The transmitted energy is measured at pressures of 1 atm and 10 atm. A higher transmission is seen at atmospheric pressure, indicating that at this pressure the absorption is saturated. Generally with a few torr of SF_6 the absorption at 10 atm is so strong that no transmitted energy is recorded. By successively pumping the cell down to 1 atm and pressurizing to 10 atm data can be taken with a range of transmission values.

4.4 Experimental Data

In Fig. 28 oscilloscope traces are shown of (a) the undistorted and (b, c) bloomed laser pulses obtained by monitoring the on-axis focal plane intensity. The characteristics of the laser pulse and other pertinent experimental parameters required for the quantitative analysis of the thermal blooming data are given in Table I. The pulses used were nominally of ~ 0.16 J energy and ~ 3 μsec duration as can be seen in Fig. 28-a. In parts b and c of Fig. 28 the blooming is produced by the addition of small amounts of SF_6 to air and He, respectively. Since SF_6 is a very strong absorber at 10.6 μ (e.g., $\alpha \sim 35$ m^{-1} for 1 torr SF_6 in air at 1 atm total pressure[18]) only small quantities were required leaving the properties of the background gases (air or He) essentially unchanged. To avoid saturation of the SF_6 absorption the total cell pressure was increased to ~ 150 psig. The use of air and helium as background gases provided a convenient method of changing the time regimes of the blooming while using the same ~ 3 μ sec pulse since the sound velocities differ by a factor of ~ 2.92 in the two gases. Thus, taking the 1/e beam radius of 0.85 mm at the cell exit window we obtain for the acoustic transit times the values of $t_h \sim 2.46$ and 0.84 μsec for air and He, respectively. The blooming in the air case is then largely in the short time regime while with He the long time blooming case should be observed.

Evidence of the thermal blooming or beam spreading, which reduces the on-axis intensity after sufficient energy has been absorbed by the gas, is shown by the narrowing or decrease in amplitude of the later portions of the pulses in Fig. 28-b,c relative to the undistorted case in a. In Fig. 29 the relative peak intensity versus time is plotted for the two bloomed pulses in Fig. 28. The data was obtained by normalizing the bloomed pulse amplitudes with the undistorted values at 0.25 μsec time increments and the absolute values were than determined by extrapolating the curves to $I_{REL} = 1.0$ at $t = 0$. The results in Fig. 29 show, as expected, that the blooming in air and helium are characteristic of the short and long-time limit cases,

respectively. The differences between the shapes of the measured I_{REL} curves and the theoretical curves in Fig. 26 are, no doubt, at least partially due to the temporal pulse shape which was far from being uniform as assumed in the theory. Also, in the so-called short-time blooming case in air, the pulse width t_p is comparable with the acoustic time t_h, which is certainly outside the region of validity for the perturbation solution and requires the complete numerical solution for the results to be accounted for.[17]

In summary, the transient thermal blooming experiments have shown qualitatively the advantage of the reduction of thermal distortion for pulses short compared to the acoustic transit time across the beam. The experimental parameters given in Table I along with the temporal history of the laser pulse can be used for comparison of the numerical solution of the transient thermal blooming with the experimental data.

REFERENCES

1. Kroll, N. and K. Watson, "Theoretical Study of Ionization of Air by Intense Laser Pulses", Physical Review A vol. 5, p. 1883, April 1972.

2. Canavan, G. H., W. A. Proctor, P. F. Nielsen and S. D. Rockwood, "CO_2 Laser Air Breakdown Calculations", IEEE Journal of Quantum Electronics vol. QE-8, p. 564, June 1972.

3. Smith, D. C., P. J. Berger, R. T. Brown and M. C. Fowler, "Investigation of Gas Breakdown with 10.6 Micron Wavelength Radiation" Air Force Weapons Laboratory Technical Report. AFWL-TR-72-182, February 1973.

4. Marquet, L.C., R. J. Hull and D. E. Lencioni, "Study in Breakdown in Air Induced by a Pulsed CO_2 Laser. IEEE Journal of Quantum Electronics, vol. QE-8 p. 564, June 1972.

5. Gebhardt, F. G. and D. C. Smith, "Self-Induced Thermal Distortion in the Near Field for a Laser Beam in a Moving Medium", IEE Journal of Quantum Electronics vol. QE-7, p. 63, February 1971.

6. Gebhardt, F. G. and D. C. Smith, "Effects of Diffraction of the Self-induced Thermal Distortion of a Laser Beam in a Crosswind", Applied Optics, vol. 11, p. 244, February 1972.

7. D. Spencer, "Absorption of DF Laser Radiation by Atmospheric Gases", Aerospace Corp. Private Communication.

8. Smith, D. C., R. T. Brown, F. G. Gebhardt, and P. J. Berger, "Effects of Particulate Matter on Atmospheric Propagation of CO_2 Laser Radiation," Semi-annual Report ONR Contract No. N00014-72-C-0469, January 1973.

9. Plass, G. N., "Mie Scattering and Absorption Cross Sections for Absorbing Particles", Appl. Opt., 5, 279 (February 1966).

10. Nielsen, P. E., and G. H. Canavan, "Interaction of High-Intensity Lasers with Optically Thin Aerosols," AFWL Laser Division Digest, LRD-71-1, June 1971.

11. Chang, D. B., J. E. Drummond and R. B. Hall, "High-Power Laser Radiation Interaction with Quartz", J. Appl. Phys. 41, 4851 (1970).

12. Gebhardt, F. G. and D. C. Smith, "Investigation of Self-Induced Thermal Effects of CO_2 Laser Radiation Propagating in Absorbing Gases", Annual Report, U. S. Army Electronics Command Report No. DAAB07-70-C-0204, April 1971.

REFERENCES CONTINUED

13. Bhattacharjie, A., "Extinction of Light by Atmospheric Aerosols in the 3.5 μ to 11.0 μ Wavelength Region - A simple Analytical Solution", United Aircraft Research Laboratories Report K-170421-1, August 1971.

14. Lencioni, D. E., "The Effect of Dust on 10.6-μm Laser-Induced Air Breakdown", Appl. Phys. Letters, vol. 23, p. 12, July 1973.

15. Hodges, J. A., "Aerosol Extinction Contribution to Atmospheric Attenuation in Infrared Wavelengths", Applied Optics, vol. 11, p. 2304, October 1972.

16. Kleiman, H. and R. W. O'Neil, "Thermal Blooming of Pulsed Laser Radiation", Appl. Phys. Letters, vol. 23, p. 43, July 1973.

17. Ulrich, P. B., "Wave Optics Calculation of Pulsed Laser Propagation in Gases," NRL Report 7413, June 7, 1972; P. B. Ulrich, "Requirements for Experimental Verification of Thermal Blooming Computer Results," J. Opt. Soc. Am. vol. 63, p. 897, July 1973.

18. Anderson, J. D., Jr., J. L. Wagner, and J. Knott, "CO_2 Laser Radiation Absorption in SF_6-Air Boundary Layers," Naval Ordnance Laboratory Report NOLTR 72-172, 1 August 1972.

TABLE I

Experimental Parameters

Cell Length L = 101 cm
Total Pathlength to Detector z = 108 cm

Absorbing Medium:
(Fig. 28b) SF_6 + Air at 11.2 atm; $\alpha L = 1.4$
(Fig. 28c) SF_6 + He at 7.8 atm; $\alpha L = 1.3$

Focused Beam 1/e Spot Diameters:

Cell Entrance	0.5 cm
Cell Exit	0.17 cm
Pulse Energy	0.16 J
Peak Power	0.2 MW

Piecewise Pulse Times*

Risetime	t_1	0.25 μsec
	t_2	0.8 μsec
Total Duration	t_3	3.0 μsec

*Piecewise Pulse

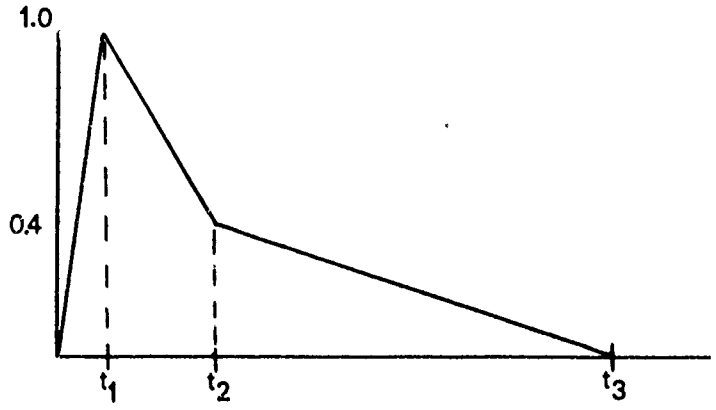

FIGURES

FIGURES CONTINUED

MAXIMUM VAPOR VELOCITY AND VAPOR TEMPERATURE VS INTENSITY PARAMETER G_1 – SEDOV MODEL

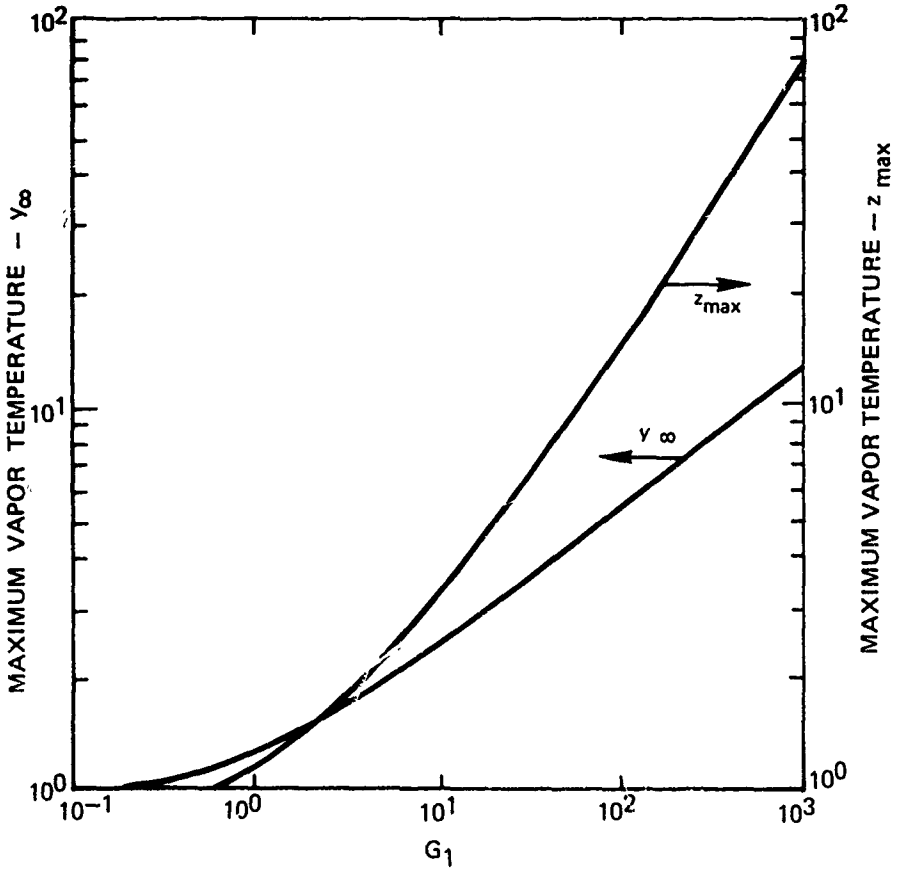

FIG. 2

EXPANDING VAPOR PROPERTIES VS DIMENSIONLESS TIME w – MODIFIED SEDOV MODEL

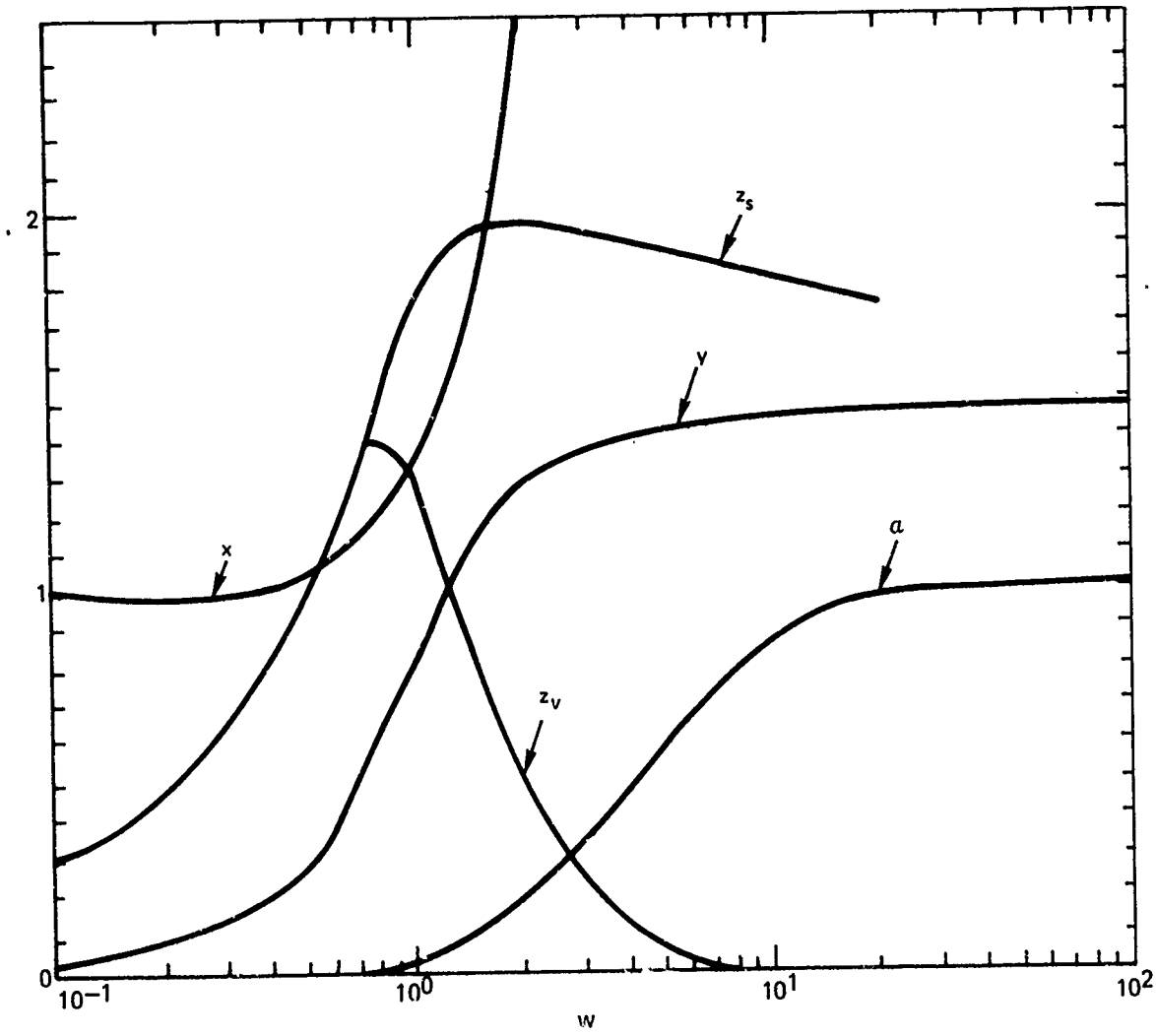

FIG. 3

MAXIMUM VAPOR VELOCITY, MAXIMUM VAPOR TEMPERATURE, AND MAXIMUM SURFACE TEMPERATURE VS INTENSITY PARAMETER G_1 FOR QUARTZ – MODIFIED SEDOV MODEL

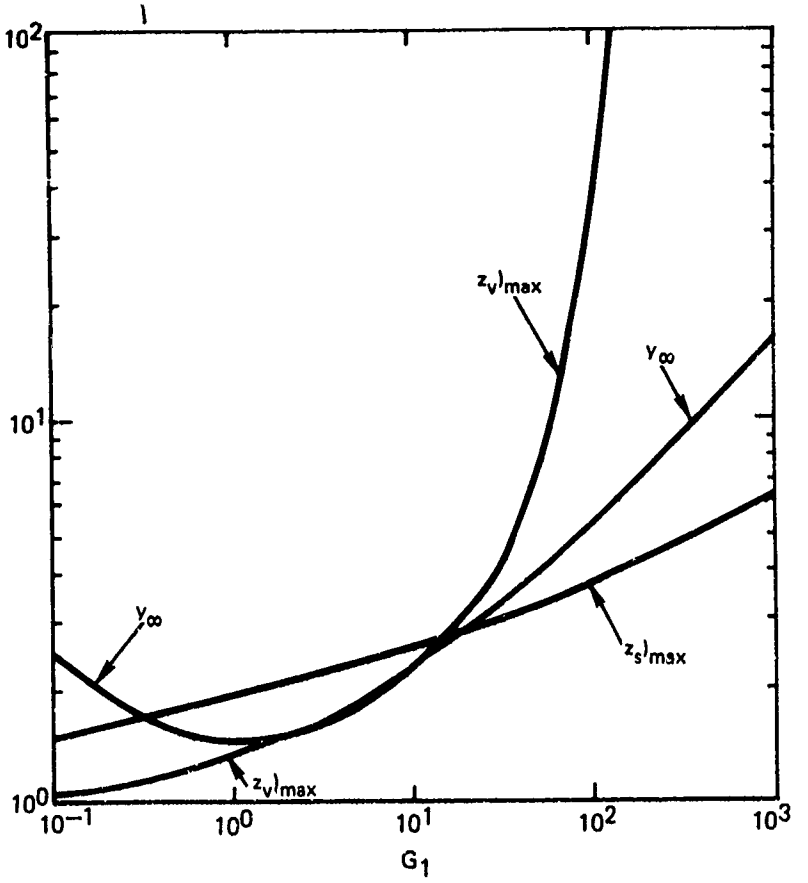

MAXIMUM VAPOR VELOCITY, MAXIMUM VAPOR TEMPERATURE, AND MAXIMUM SURFACE TEMPERATURE VS INTENSITY PARAMETER G_1 FOR CARBON – MODIFIED SEDOV MODEL

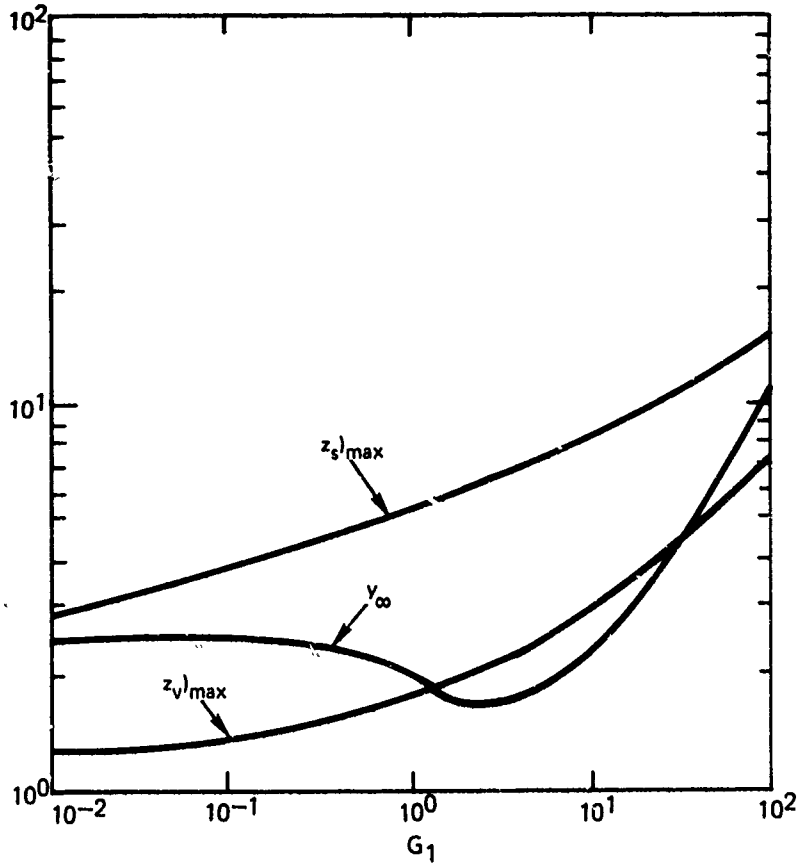

FIG. 5

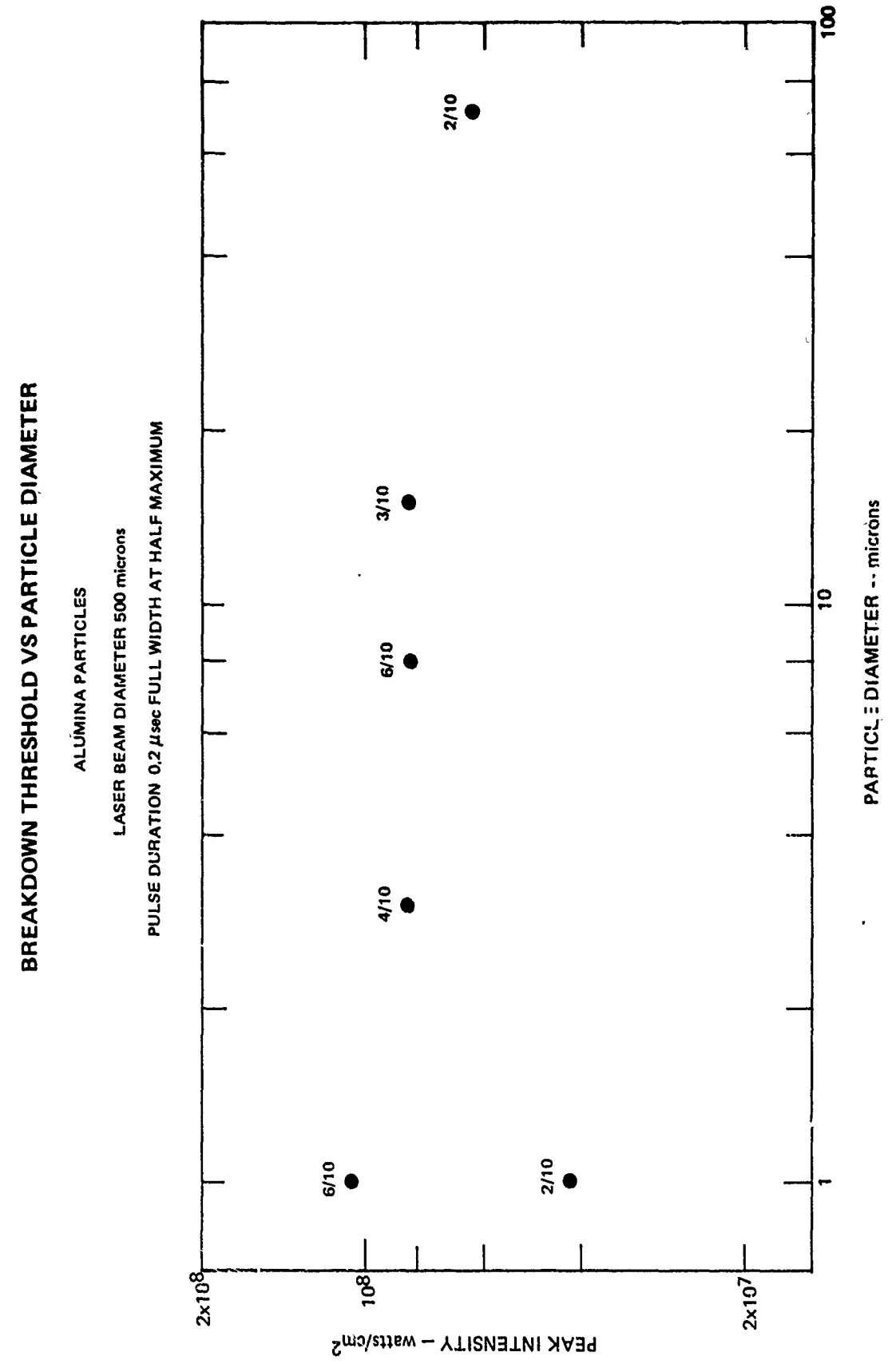
BREAKDOWN THRESHOLD VS PARTICLE DIAMETER
ALUMINA PARTICLES
LASER BEAM DIAMETER 500 microns
PULSE DURATION 0.2 μsec FULL WIDTH AT HALF MAXIMUM
PEAK INTENSITY – watts/cm²
2x10⁸
10⁸
2x10⁷
1
10
100
PARTICLE DIAMETER – microns
6/10
2/10
4/10
6/10
3/10
2/10

FIG. 6

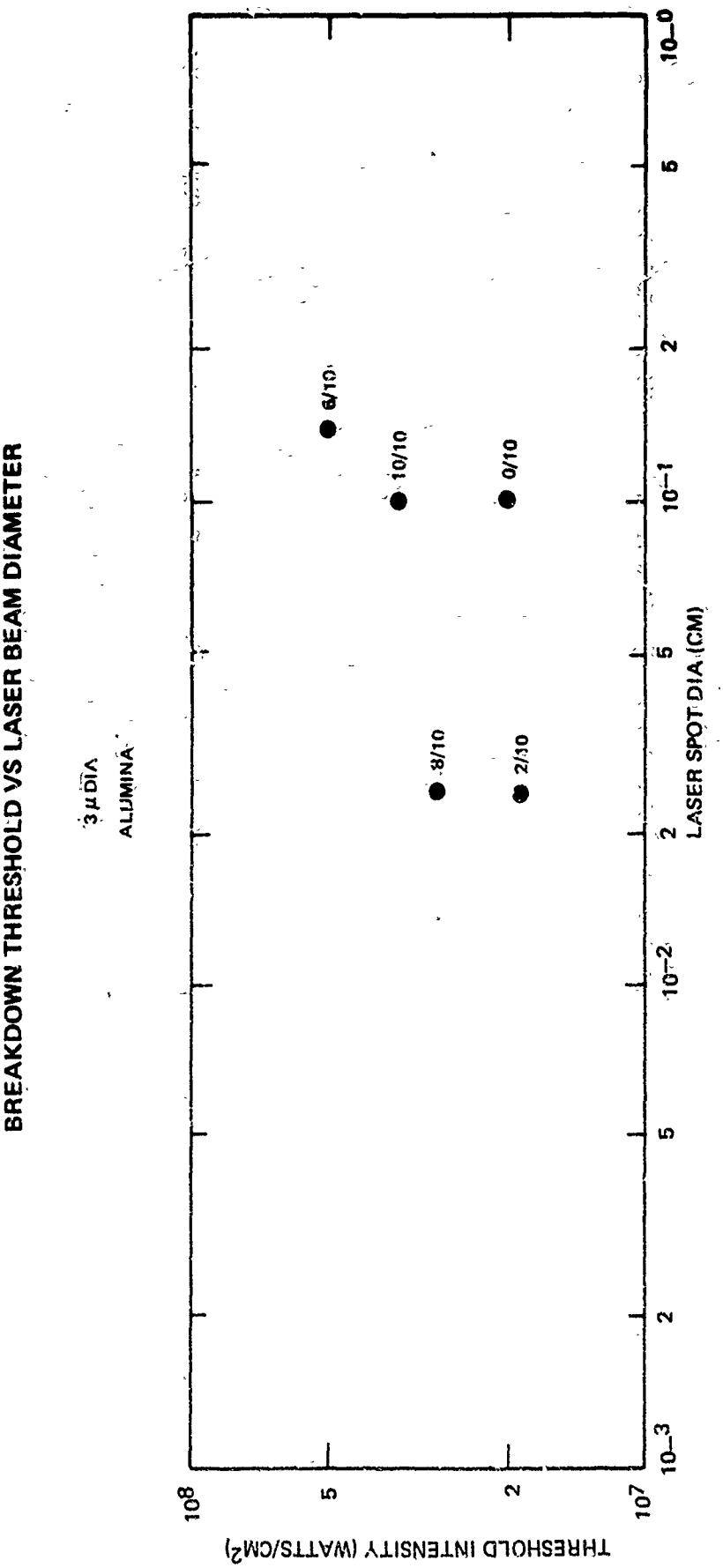
BREAKDOWN THRESHOLD VS LASER BEAM DIAMETER
3 μ DIA
ALUMINA
6/10
10/10
0/10
8/10
2/10
THRESHOLD INTENSITY (WATTS/CM2)
LASER SPOT DIA (CM)
10^8
5
2
10^7
10^-3
2
5
10^-2
2
5
10^-1
2
5
10^0

FIG. 7

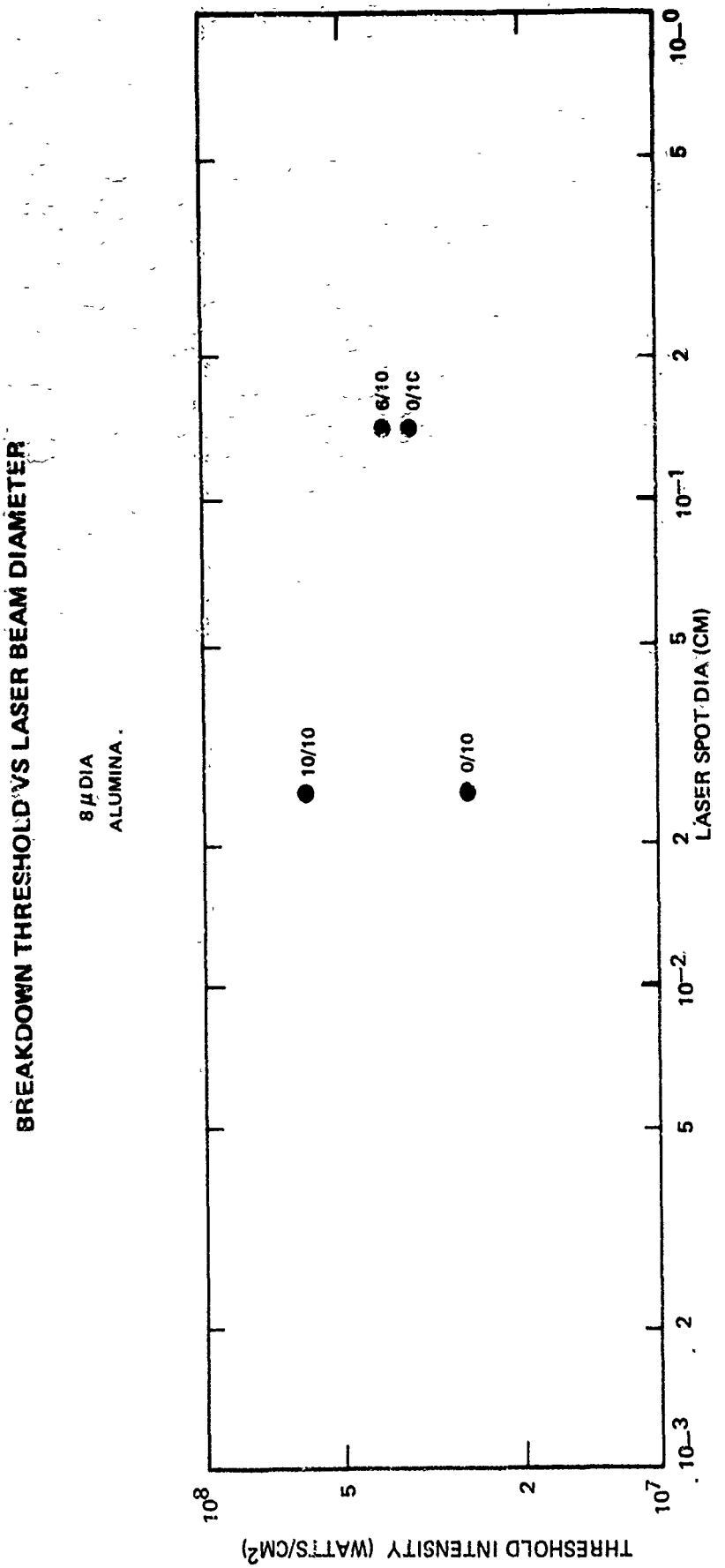
BREAKDOWN THRESHOLD VS LASER BEAM DIAMETER
8 μ DIA
ALUMINA
10/10
0/10
6/10
0/10
THRESHOLD INTENSITY (WATTS/CM²)
LASER SPOT DIA (CM)
10⁸
5
2
10⁷
10⁻³
2
5
10⁻²
2
5
10⁻¹
2
5
10⁻⁰

FIG. 8

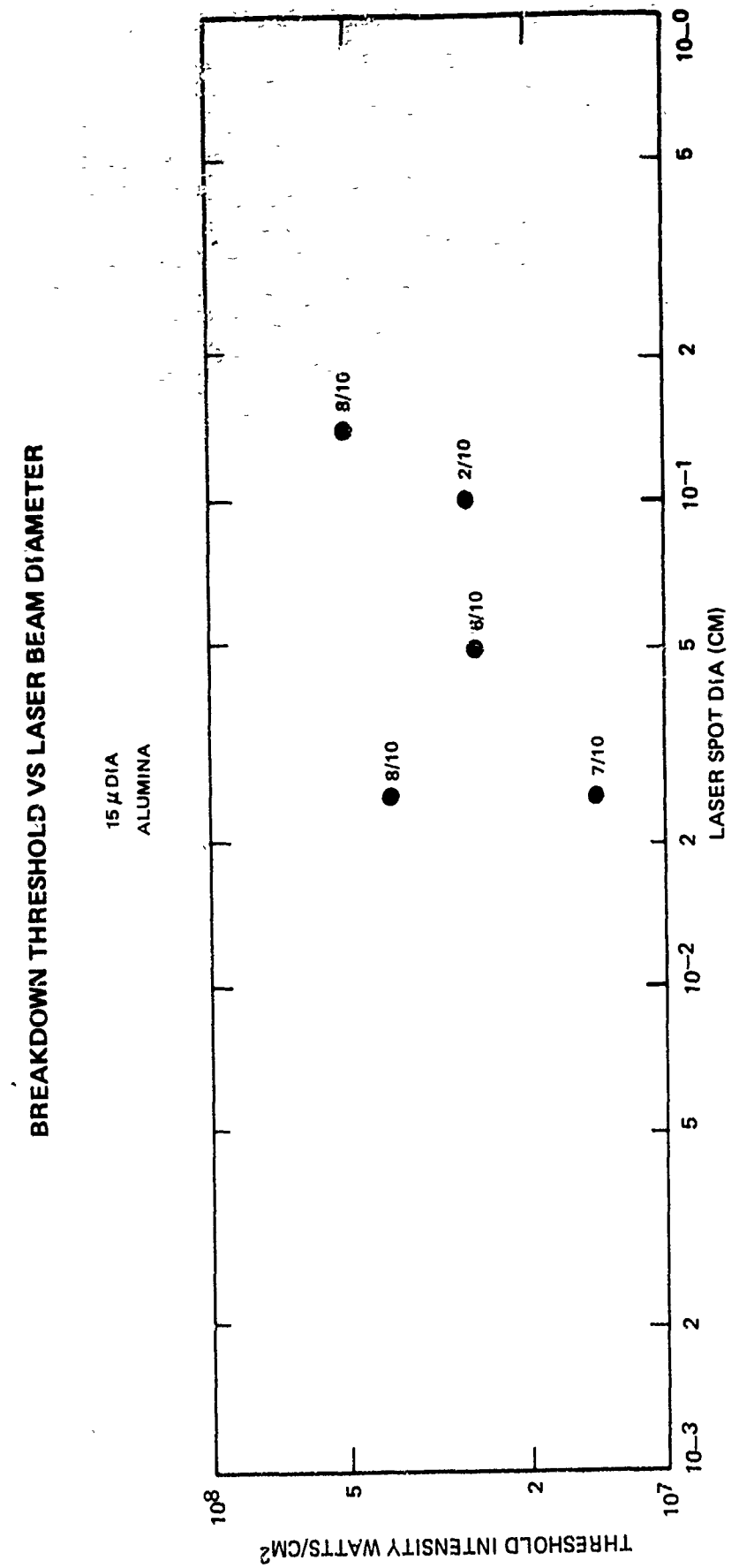
BREAKDOWN THRESHOLD VS LASER BEAM DIAMETER
15 μ DIA
ALUMINA
8/10
8/10
2/10
6/10
7/10
THRESHOLD INTENSITY WATTS/CM²
LASER SPOT DIA (CM)
10⁸
5
2
10⁷
10⁻³
2
5
10⁻²
2
5
10⁻¹
2
5
10⁰

FIG. 9

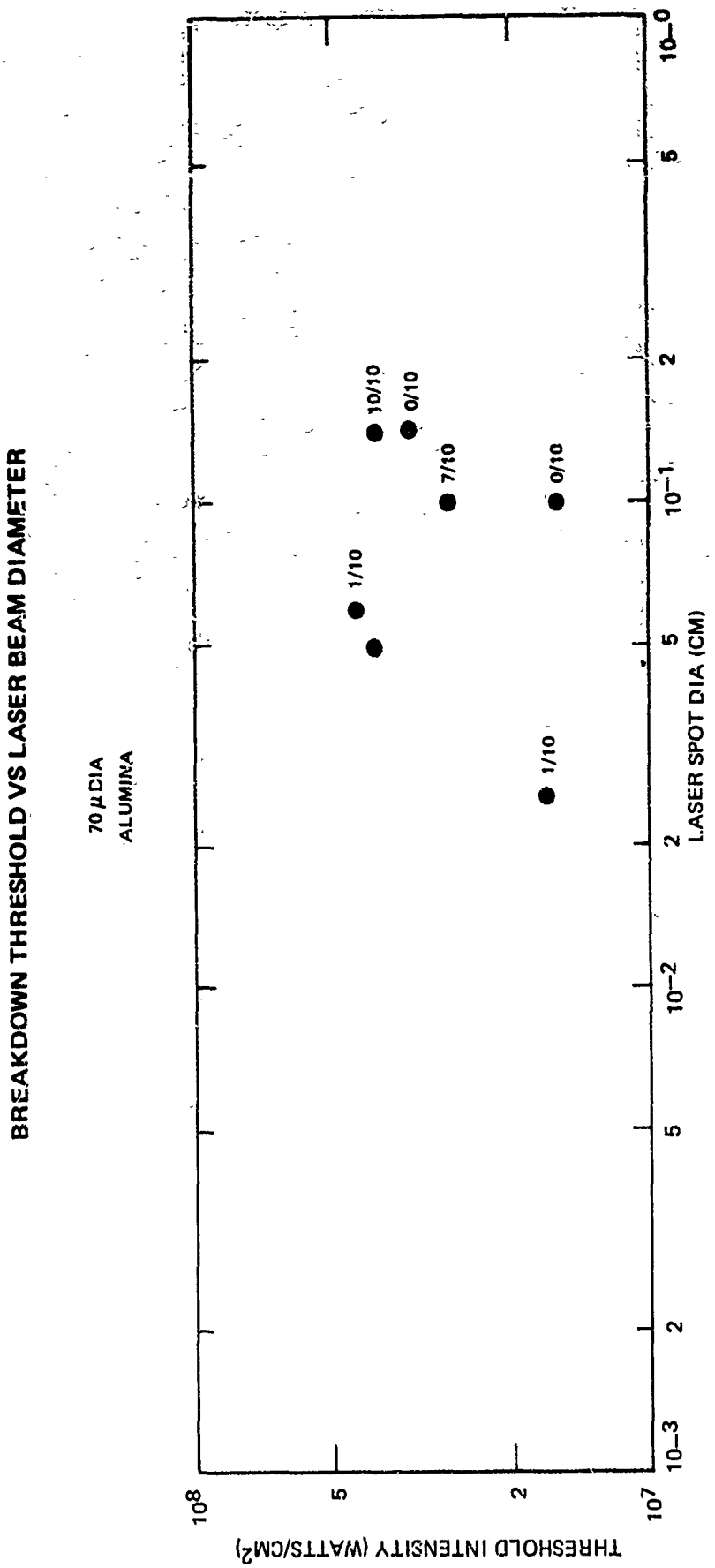
BREAKDOWN THRESHOLD VS LASER BEAM DIAMETER
70 μ DIA
ALUMINA
1/10
10/10
0/10
7/10
0/10
1/10
THRESHOLD INTENSITY (WATTS/CM2)
LASER SPOT DIA (CM)
10^8
5
2
10^7
10^-3
2
5
10^-2
2
5
10^-1
2
5
10^0

FIG. 10

BREAKDOWN THRESHOLD AS A FUNCTION OF BACKGROUND AIR PRESSURE

50μ DIA. PARTICLES
10.6μ WAVELENGTH RADIATION

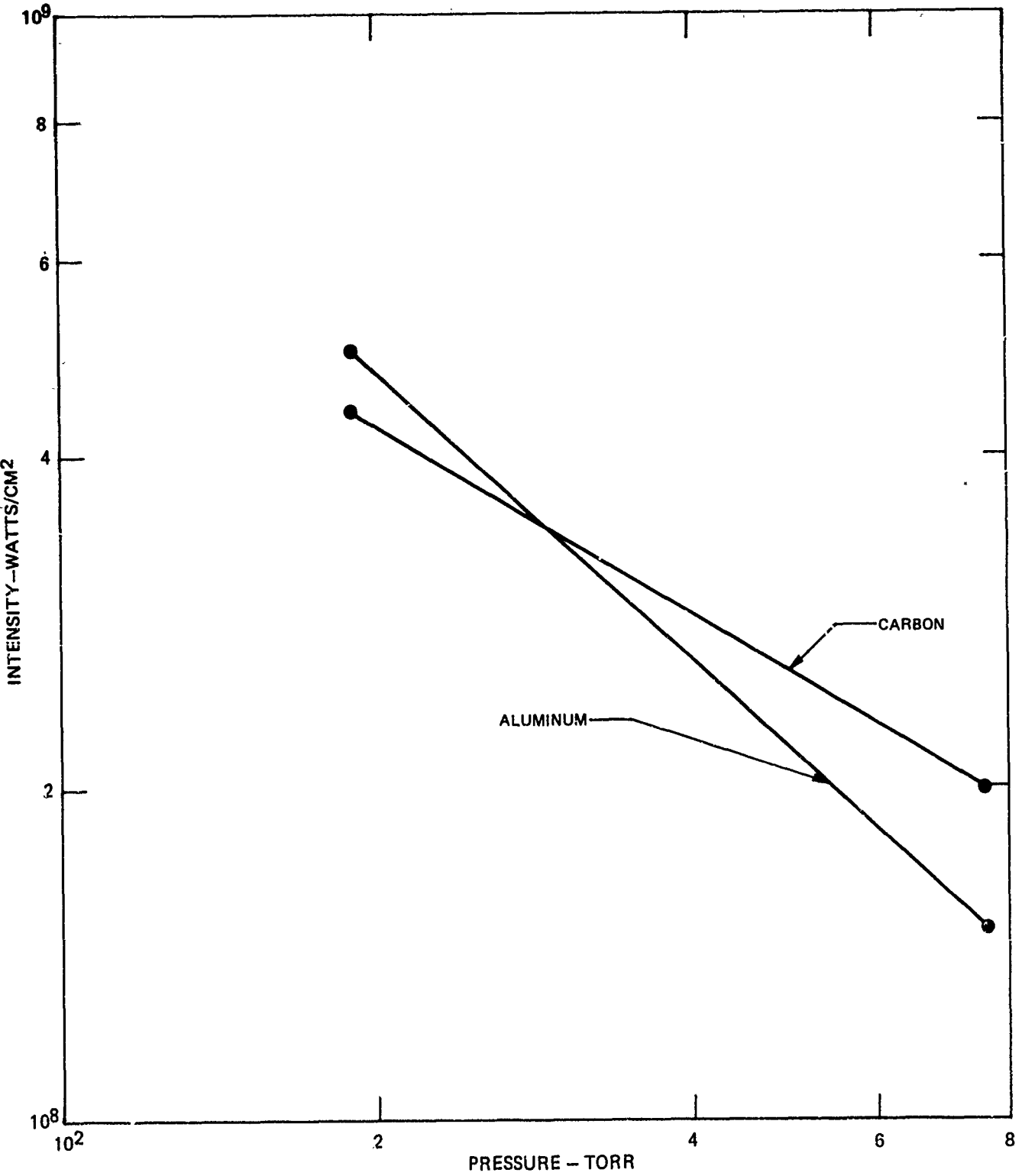

FIG. 11

STREAK PHOTOGRAPH OF PARTICLE INDUCED GAS BREAKDOWN

50 μ DIA ALUMINUM PARTICLE

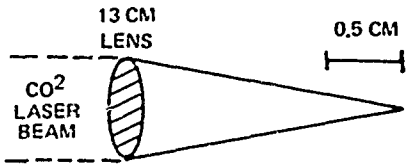

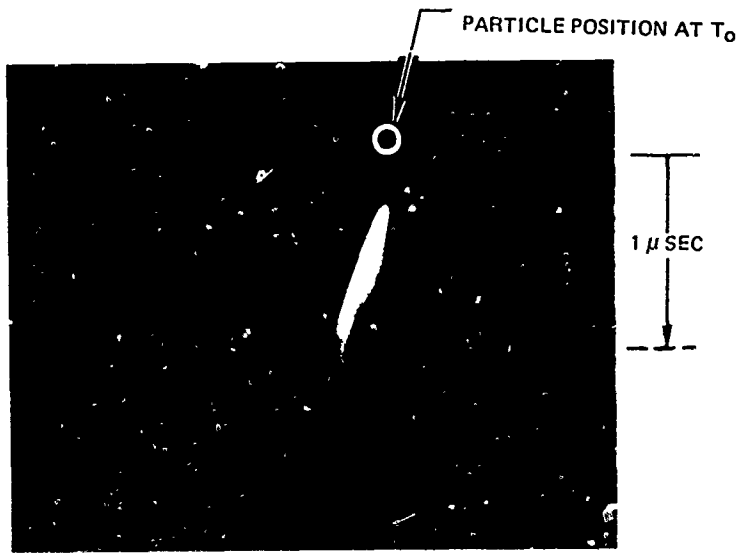

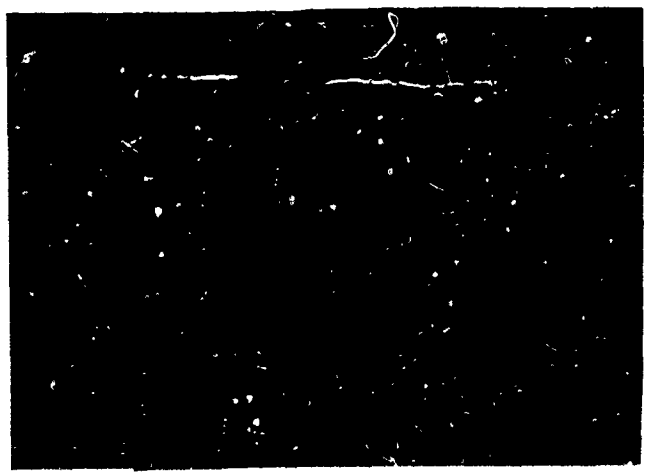

LASER PULSE INTENSITY
$I_{MAX} = 0.8 \times 10^9$ WATTS/CM^2

STREAK CAMERA
RAMPING VOLTAGE

T_o | 1 μ SEC/DIV

FIG. 12

STREAK PHOTOGRAPH OF WIRE INDUCED BREAKDOWN

250μ DIA STEEL WIRE

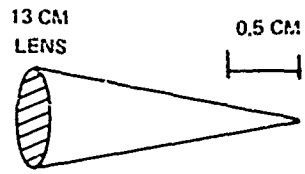

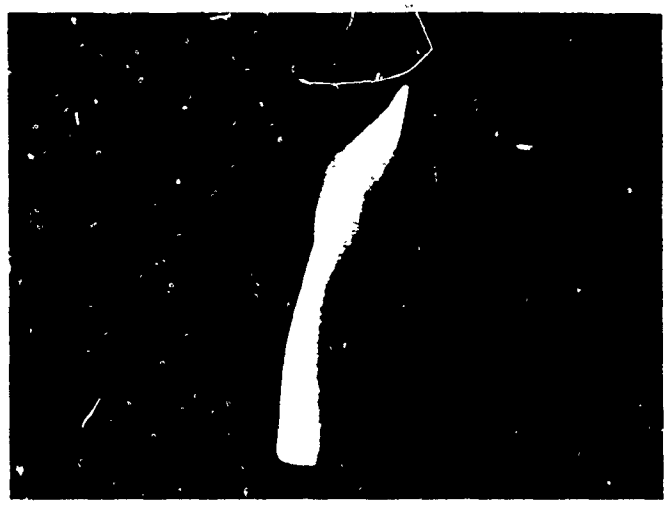

1μSEC

T_0 | 1μSEC/DIV

LASER INTENSITY
$I_{MAX} = 0.8 \times 10^9$ WATTS/CM^2

STREAK CAMERA
RAMP VOLTAGE

FIG. 13

STREAK PHOTOGRAPH OF PARTICLE INDUCED GAS BREAKDOWN

50μ DIA ALUMINUM PARTICLE

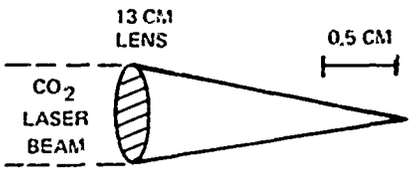

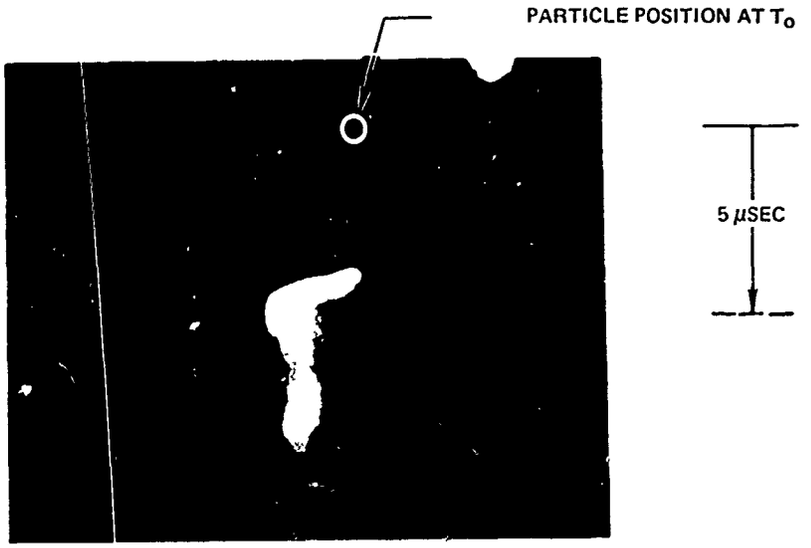

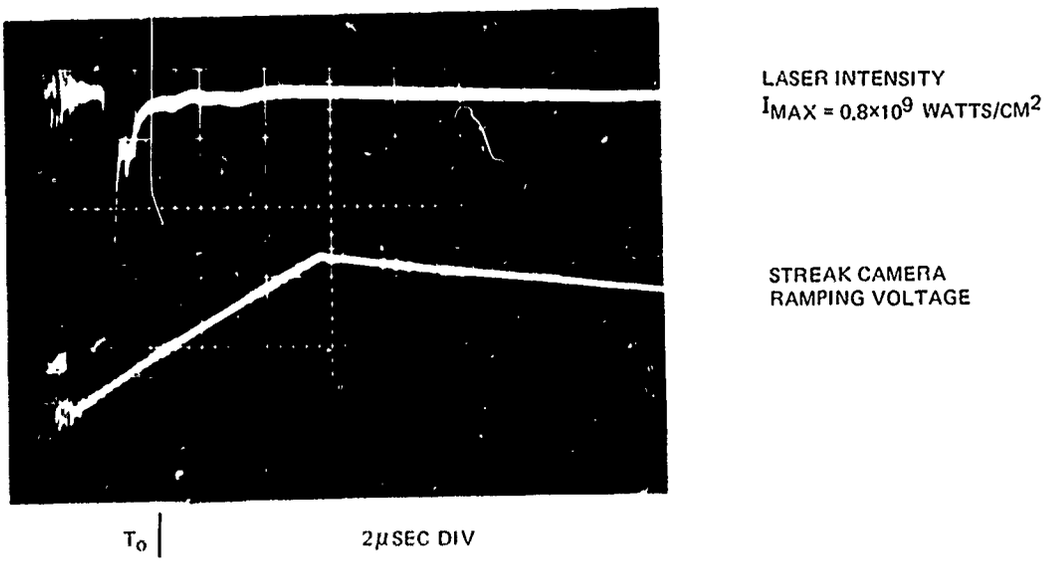

FIG. 14

STREAK PHOTOGRAPH OF PARTICLE INDUCED GAS BREAKDOWN

50 μ DIA SALT PARTICLE

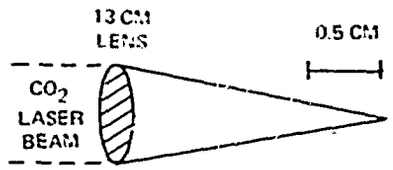

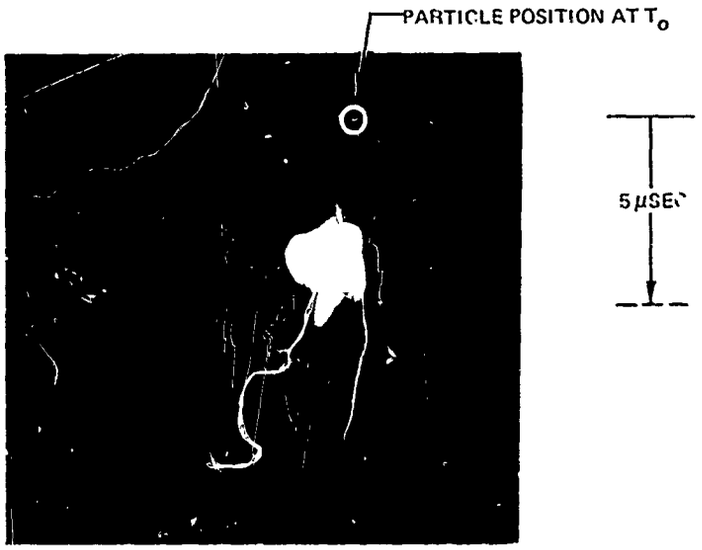

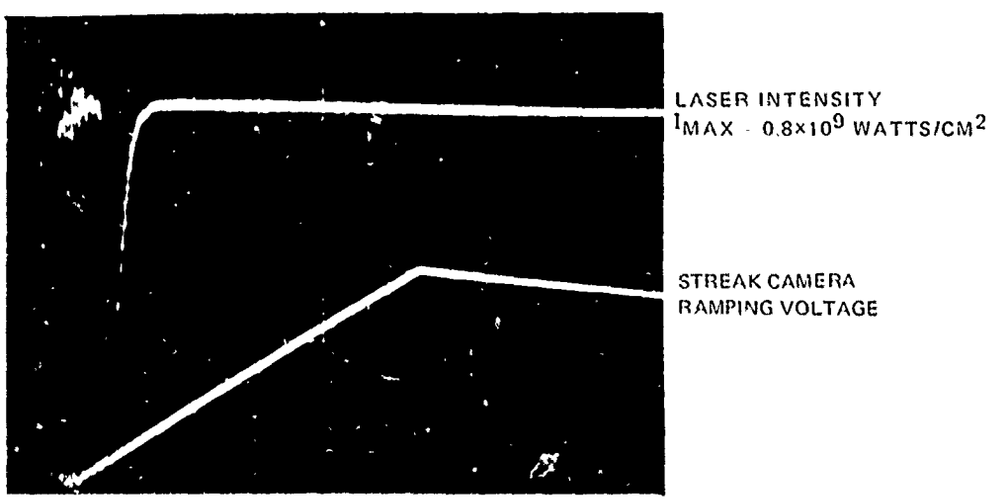

FIG. 15

PARTICLE SUSPENSION APPARATUS AND SCHLIEREN SYSTEM

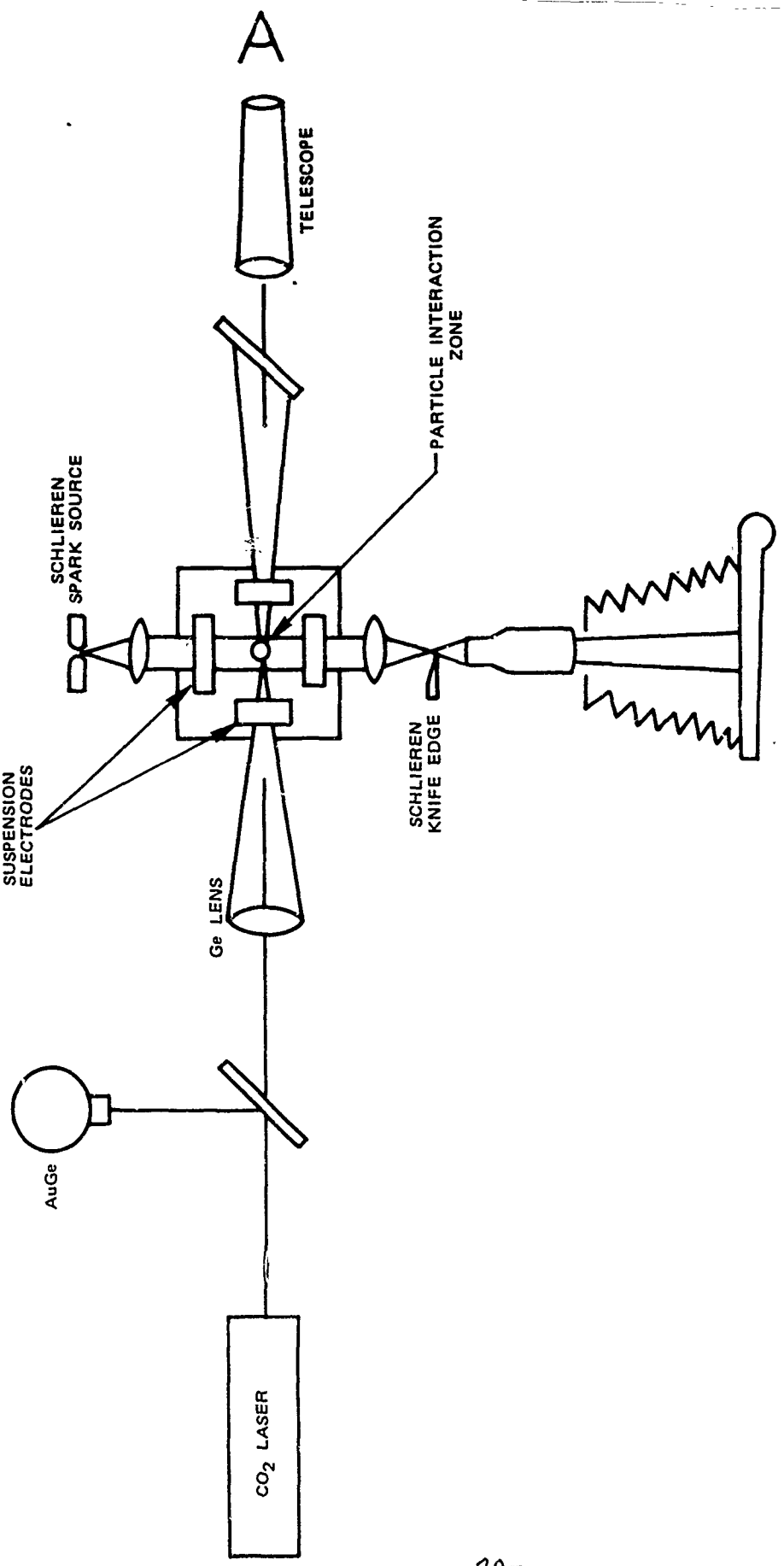

FIG. 16

PULSED LASER — PARTICLE HEATING

SINGLE 50μ CARBON PARTICLES

τ_d = 0.5μsec d = 6.5x10^{-2} cm

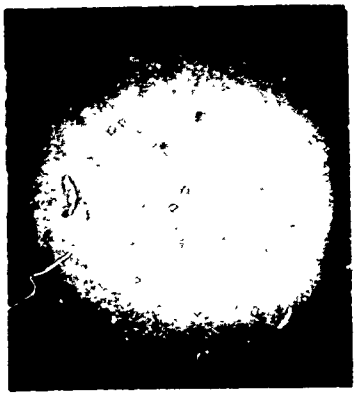

I_p = 6.0x10^7 W/cm^2

J = 11 J/cm^2

I_p = 1.0x10^8 W/cm^2

J = 19 J/cm^2

I_p = 2.4x10^8 W/cm^2

J = 44 J/cm^2

FIG. 17

CW LASER – PARTICLE HEATING

SINGLE 50 μ CARBON PARTICLES

IN STP AIR, 3×10^3 W/cm^2

τ_d = 10 msec

τ_d = 20 msec

τ_d 30 msec

FIG. 18

CW LASER – PARTICLE HEATING

SINGLE 100 μ CARBON PARTICLES

IN STP AIR, 3×10^3 W/cm^2

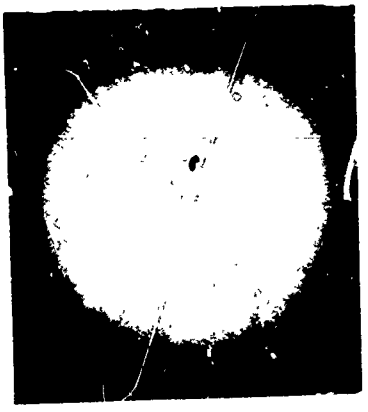

LASER OFF

τ_d = 20 msec

FIG. 19

TEMPERATURE PROFILE DEVELOPMENT IN THE ATMOSPHERE WITH PARTICLE ABSORPTION OF LASER RADIATION

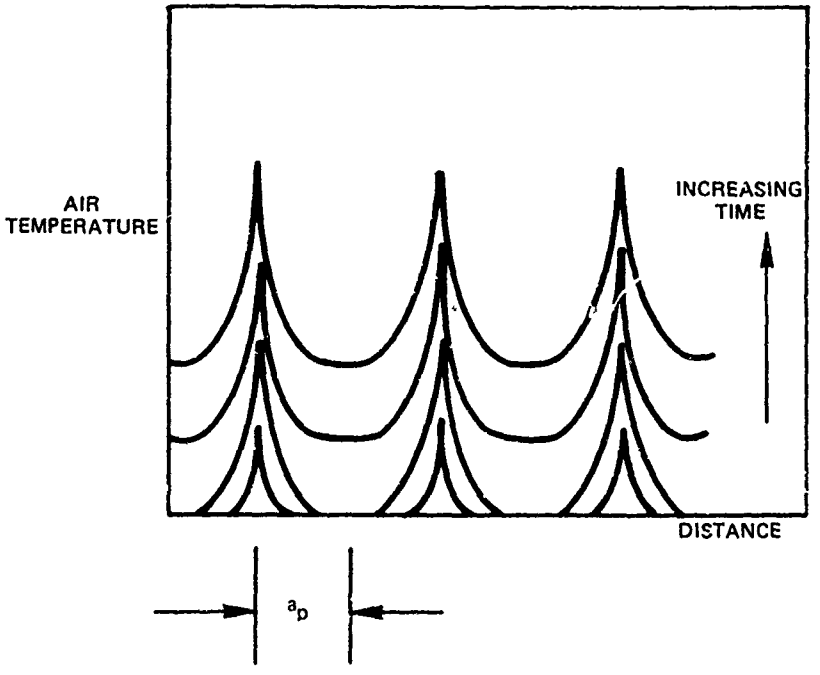

FIG. 20

PARTICLE–INDUCED THERMAL BLOOMING EXPERIMENT

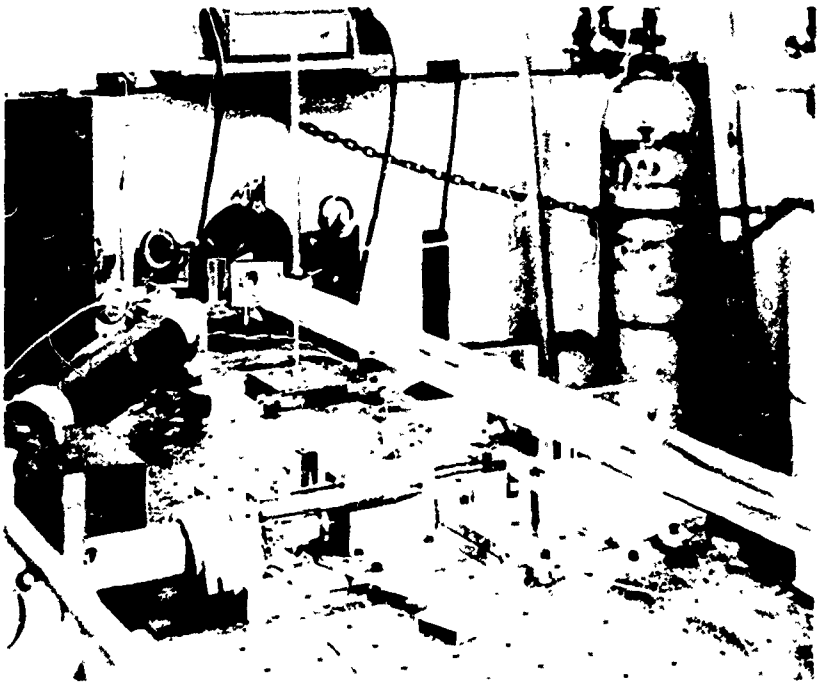

a) ABSORPTION CELL

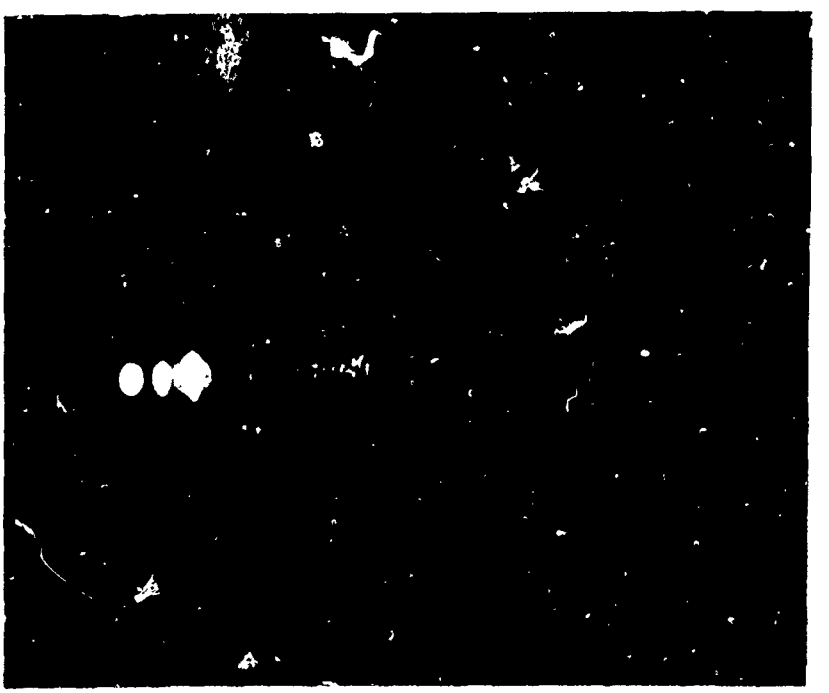

b) CARBON PARTICLES IN He Ne BEAM

FIG. 21.

BEAM PROFILES FOR PARTICLE–INDUCED THERMAL BLOOMING

(NATURAL CONVECTION CASE)

UNDISTORTED BEAM

DISTORTED BEAM

CARBON PARTICLES
IN STP AIR

$n_p \approx 10^4$ cm^{-3}

DISTORTED BEAM

CARBON PARTICLES
IN STP AIR

$n_p \approx 2 \times 10^4$ cm^{-3}

FIG. 22

BEAM PROFILES FOR PARTICLE–INDUCED THERMAL BLOOMING

(NATURAL CONVECTION CASE)

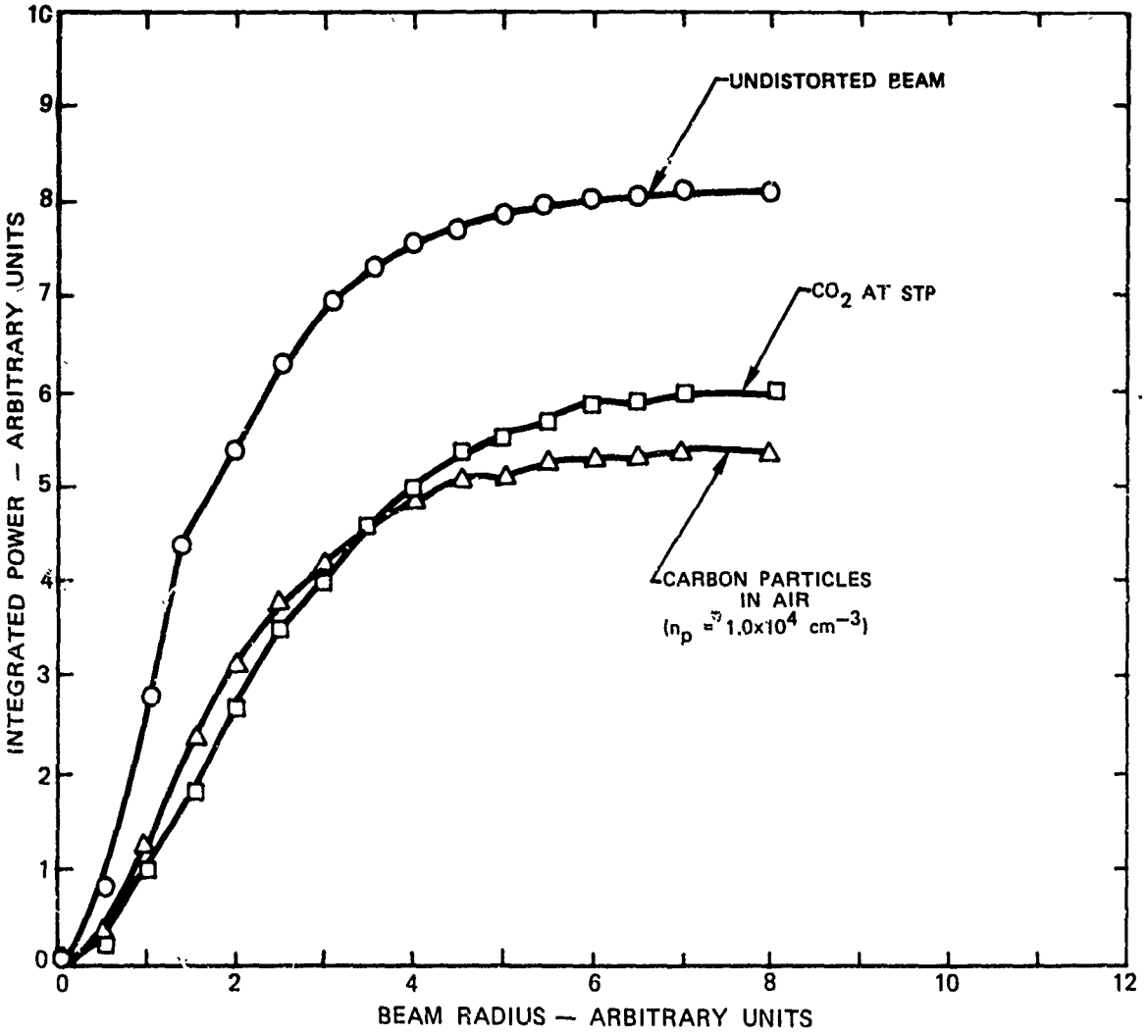

FIG. 23

CENTERLINE INTENSITY VS TIME

(BEAM SWITCHED ON AT t = 0)

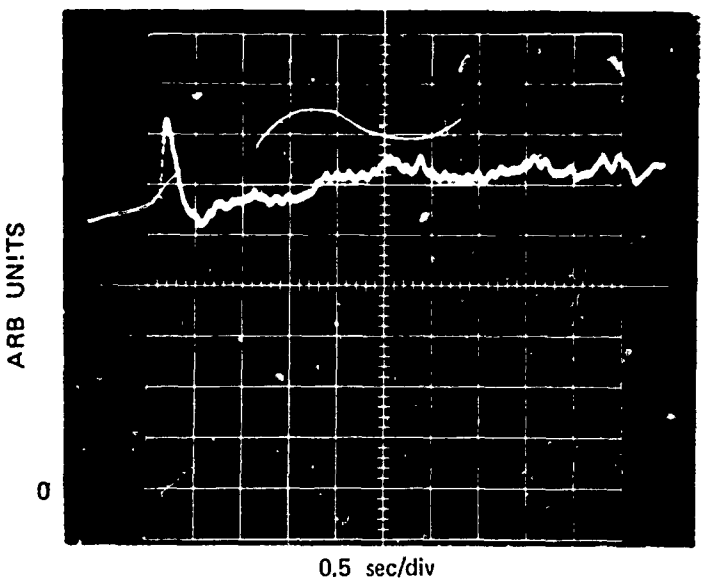

CARBON PARTICLES IN STP AIR

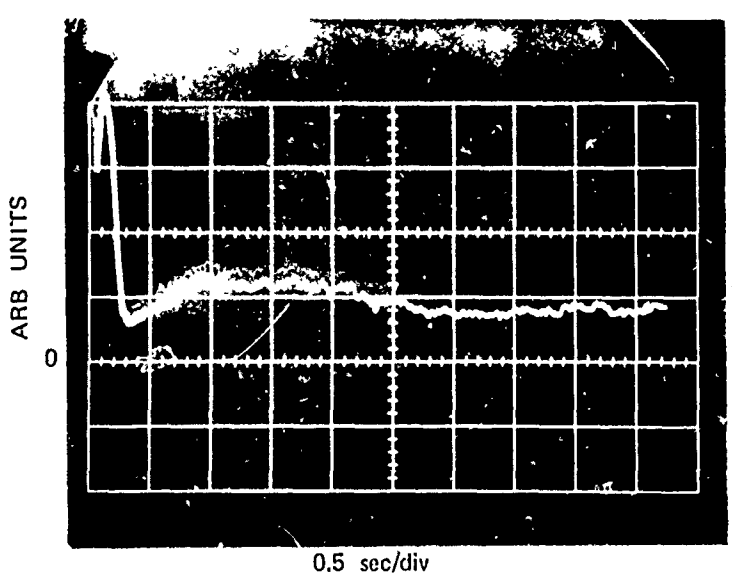

STP CO_2

FIG. 24

CARBON AEROSOL SIZE DISTRIBUTION

a) PHOTOGRAPH OF PARTICLES (50x MAGNIFICATION)

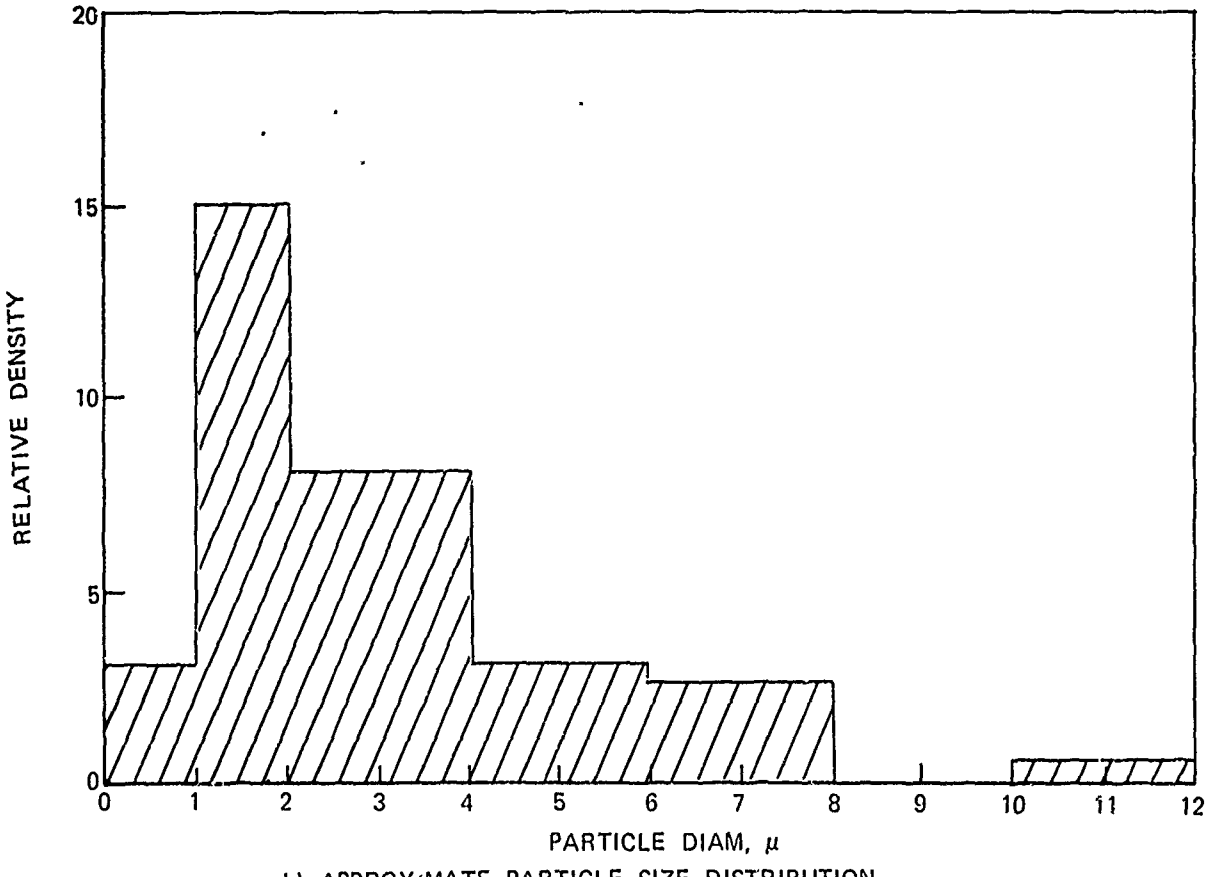

b) APPROXIMATE PARTICLE SIZE DISTRIBUTION

FIG. 25

NORMALIZED PARTICLE ABSORPTION CROSS SECTION

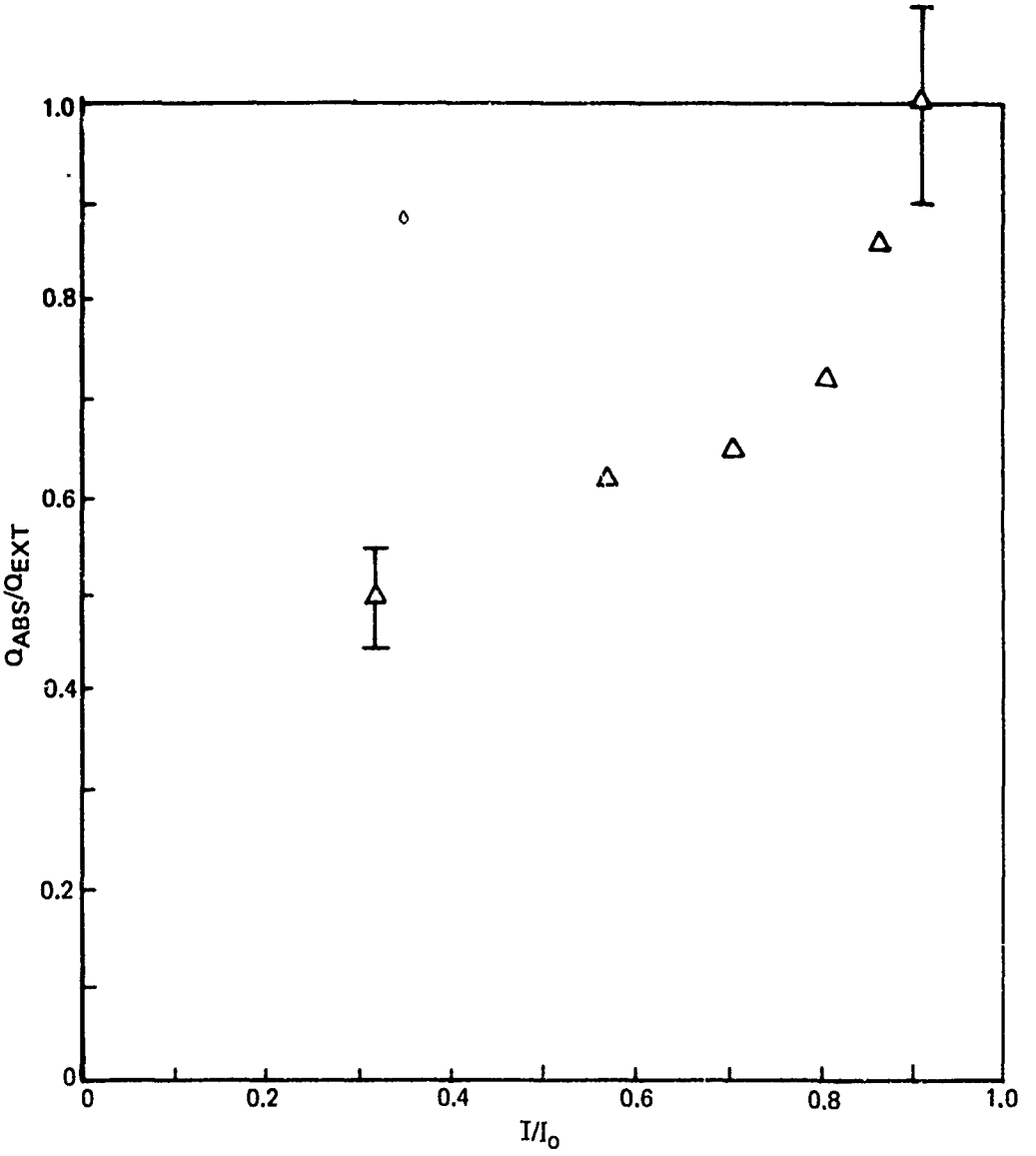

FIG. 26

RELATIVE PEAK INTENSITY VS. TIME

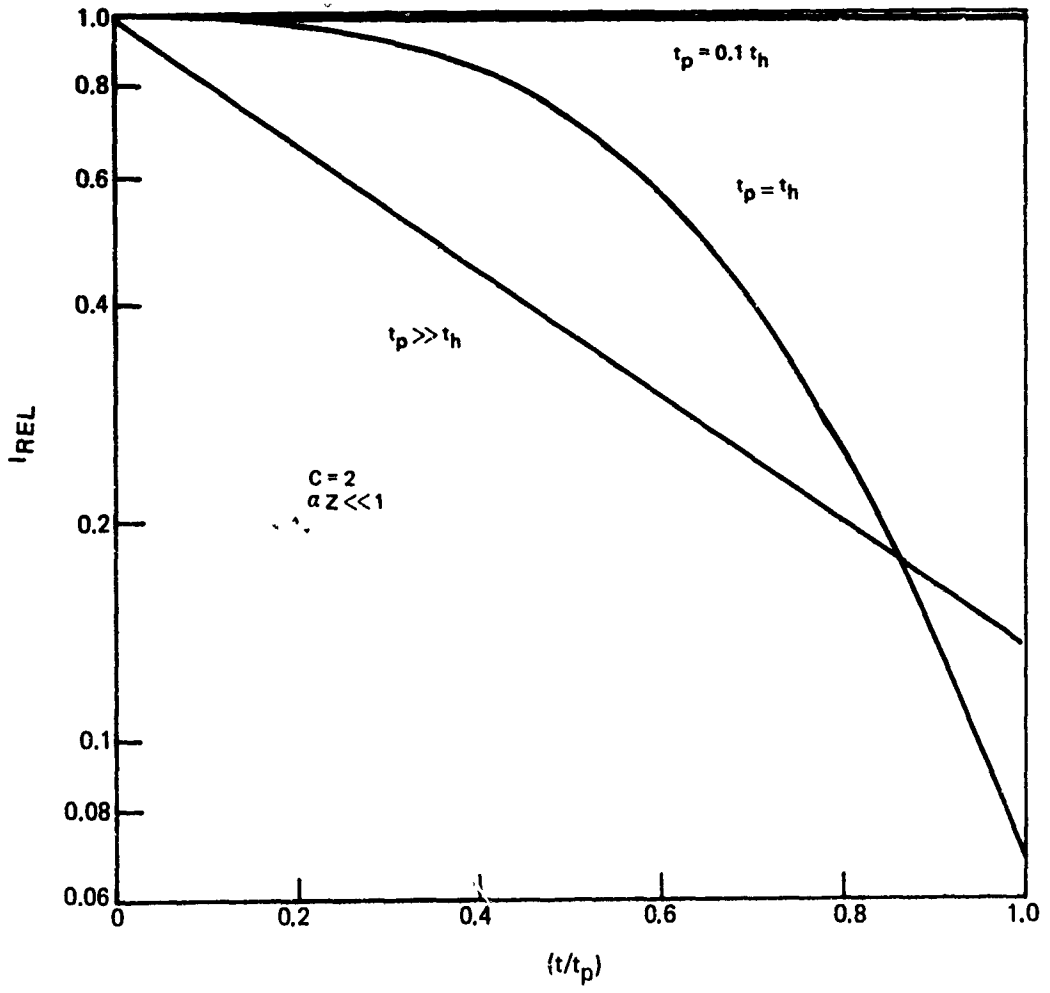

FIG. 27

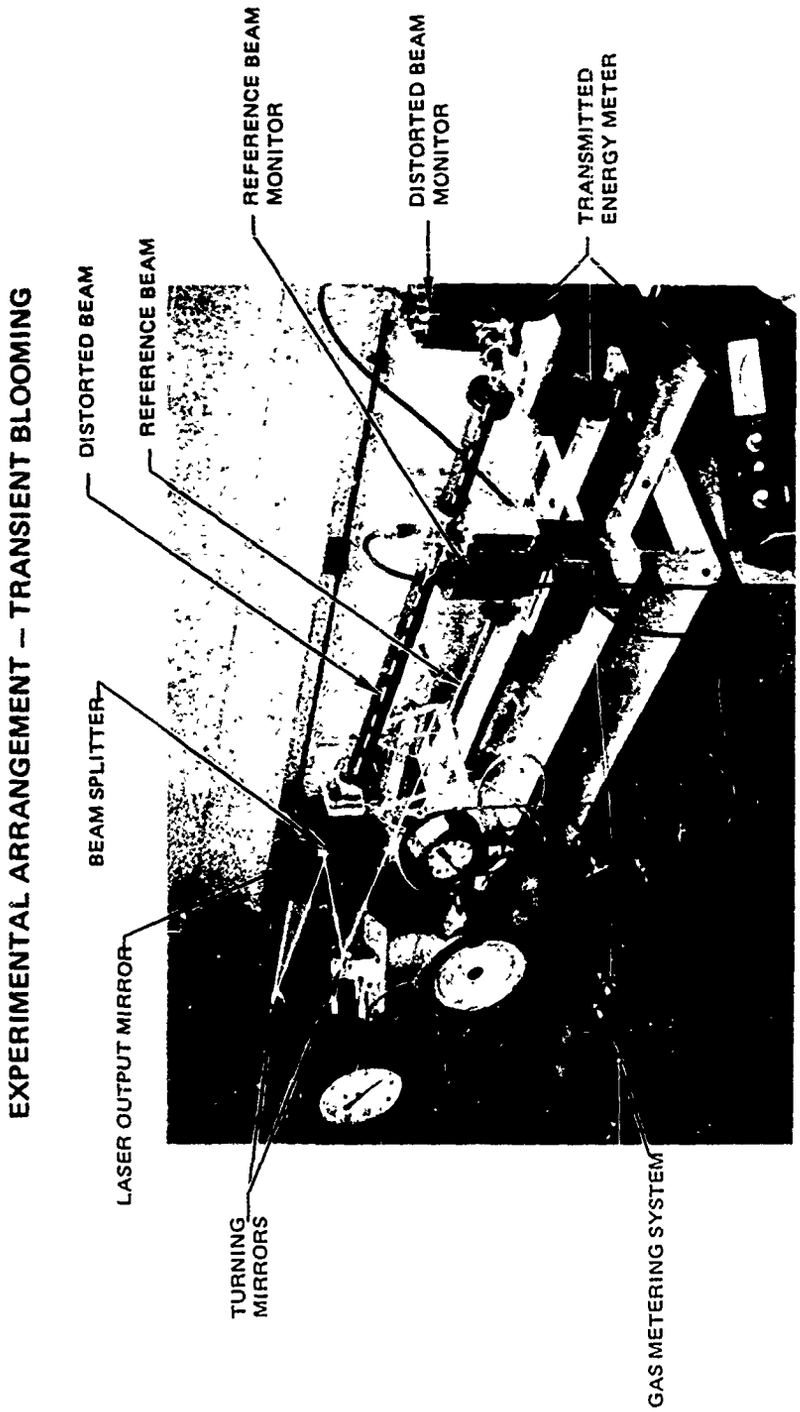
EXPERIMENTAL ARRANGEMENT – TRANSIENT BLOOMING
DISTORTED BEAM
REFERENCE BEAM
BEAM SPLITTER
LASER OUTPUT MIRROR
TURNING MIRRORS
REFERENCE BEAM MONITOR
DISTORTED BEAM MONITOR
TRANSMITTED ENERGY METER
GAS METERING SYSTEM

FIG. 28

THERMAL BLOOMED LASER PULSES

a)

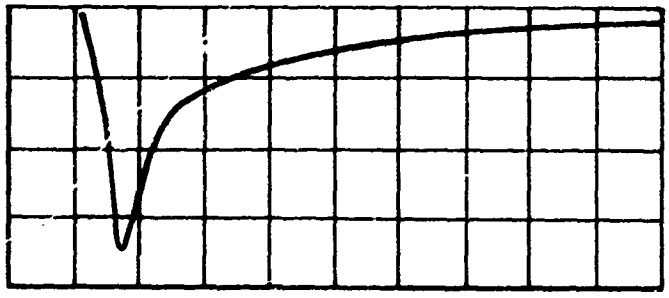

b)

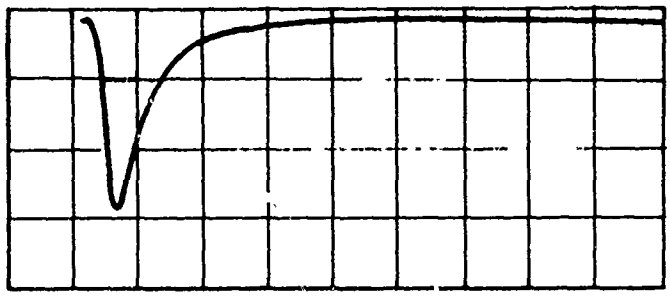

c)

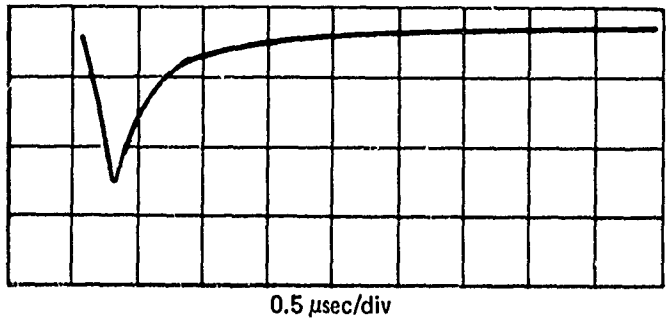

0.5 μsec/div

FIG. 29

RELATIVE PEAK INTENSITY VS. TIME